

Multilevel Asymptotic-Preserving Monte Carlo for Particle Simulations

Bert Mortier*

Pieterjan Robbe*

Abstract

We develop a novel Multilevel Asymptotic-Preserving Monte Carlo (ML-APMC) method for simulating the kinetic Boltzmann transport equation with Bhatnagar–Gross–Krook (BGK) collision operator. This equation occurs, for instance, in mathematical models of the neutral particles in the plasma edge of nuclear fusion reactors. The main features of our method are a new and improved recipe for correlating particle trajectories with different time step sizes, and a new and more general level selection strategy. We illustrate the efficiency of our ML-APMC method by applying it to a one-dimensional fusion test case with nonhomogeneous and anisotropic plasma background. Our method yields significant speedups, both in the low and high collisional regime. In the high-collisional case, our ML-APMC outperforms the single-level APMC method by several orders of magnitude.

Contents

1	Introduction	2
2	The KD simulation scheme	3
3	Correlating fine and coarse particle paths	4
3.1	Mapping the random numbers from the fine to the coarse particle path	5
3.2	Aggregating the random numbers in the coarse path	7
3.3	An algorithm for correlated KD sampling	8
4	Multilevel Asymptotic-Preserving Monte Carlo	9
4.1	Multilevel sampling	9
4.2	Level selection	12
5	Numerical results	14
5.1	Coarse particle path consistency	15
5.2	A heuristic level selection method	16
5.3	Performance of the ML-APMC method	18
6	Conclusion and future work	20

*KU Leuven, Department of Computer Science, NUMA Section.
Celestijnenlaan 200A box 2402, 3001 Leuven, Belgium.
{bert.mortier, pieterjan.robbe}@kuleuven.be}

1 Introduction

Kinetic equations play a vital role in many modern applications. For example, in mathematical models for nuclear fusion reactors such as ITER and DEMO, see [15], the physics of neutral particles in the plasma is modeled using the Boltzmann transport equation (BTE) with Bhatnagar–Gross–Krook (BGK) approximation, see, e.g., [2, 17, 26]. The kinetic equation then boils down to simulating each and every individual collision of the neutral particle with the plasma background. Near the plasma edge, there is an area of increased neutral-plasma collision rates. This reduces the heat load on the the plasma-facing components significantly. However, the increase in the number of collisions has severe implications on the computational burden of the kinetic description. On the other hand, it is well-known that, in the high-collisional limit, the behavior of the neutral particles converges to an advection-diffusion process, see, e.g., [20]. The latter can be simulated cheaply using random walks.

Thus, there are regions in the domain where a kinetic description is required, and also regions with a high collision rate where this kinetic description becomes intractable, but where a diffusive approximation exists that is cheap to simulate. Domain decomposition is the method of choice for solving these type of problems, see, e.g. [4, 7]. However, the domain decomposition approach requires a good partitioning of the domain into a kinetic and a diffusive part, and an efficient coupling between both. An alternative hybrid approach, that avoids this coupling altogether, are so-called *Asymptotic-Preserving Monte Carlo* (APMC) methods [23, 8]. These methods use a single approximation scheme throughout the entire domain, such that the method has the accuracy of the kinetic simulation in the low-collision regions, and the efficiency of a diffusive simulation in the high-collision regions. APMC methods were originally developed in the context of radiation transport, see, e.g., [10, 9], and later on also for neutron transport, see [3], and the Boltzmann-BGK equation, see [11].

In this paper, we present a multilevel extension of the APMC method, conveniently termed *Multilevel Asymptotic-Preserving Monte Carlo* (ML-APMC). Our method combines the asymptotic-preserving scheme from [19], the so-called kinetic-diffusion (KD) scheme, with the *Multilevel Monte Carlo* (MLMC) method, see, e.g., [12, 13]. The latter method uses a hierarchy of coarse approximations to reduce the computational cost of a simulation. In the context of particle simulations, the hierarchy of coarse approximations can be constructed by subsequently increasing the time step size in the simulation. The goal of our ML-APMC method is then to reduce the computational cost of the kinetic simulation, while keeping the flexibility of the APMC method.

Other work on combining APMC with MLMC can be found in [16]. Our current work differs from [16] in several ways. First, our multilevel method is based on a new and superior recipe to generate correlated particle trajectories with different time step sizes. Second, our APMC scheme is based on the KD scheme from [19], and not the asymptotic-preserving scheme from [8]. The latter has a computational cost that grows unbounded with decreasing time step size. Finally, we apply our method to the more relevant case of a nonhomogeneous plasma background, and show that our method can be applied without change to an anisotropic plasma background.

The remainder of this text is organized as follows. First, in Section 2, we briefly discuss the APMC scheme from [19]. Next, in Section 3, we present the main contribution of this work, i.e., the improved recipe for correlating particle trajectories. In Section 4, we discuss the MLMC method in the context of kinetic equations, and address the construction of an optimal hierarchy of coarse approximations for multilevel sampling. Finally, in Section 5, we present numerical results that illustrate the superiority of our ML-APMC scheme over the standard APMC method from [19] in terms of computational cost.



Figure 1: An illustration of a particle trajectory in the KD scheme. A kinetic step (—) ends with a collision (•), and is always followed by a diffusive step (····) until the end of the time step.

2 The KD simulation scheme

In this section, we discuss the kinetic-diffusion (KD) simulation scheme for the Boltzmann-BGK equation introduced in [19]. Suppose the time domain of the simulation is discretized into disjoint time intervals of equal length δt . Let $x(t)$ and $v(t)$ denote the position and velocity of a particle. In the KD simulation scheme, particles follow an alternatingly kinetic and diffusive trajectory. Particles move kinetically with a constant velocity $v(t)$, until a collision occurs. This kinetic step is oblivious to any time discretization. Then, for the remainder of the time step in which the collision occurred, the particle moves according to a random walk with identical mean and variance as the corresponding kinetic process. In the diffusive limit, where many collisions occur, the random walk corresponds to the diffusive limit of the Boltzmann-BGK equation. This diffusive step is meant to avoid the explicit simulation of a large number of collisions.

It is clear how this hybrid scheme solves the domain decomposition coupling issue: if, on average, less than one collision occurs in every time step, most of the particle trajectory will consist of kinetic steps, and the scheme correspond to the kinetic approximation of the Boltzmann-BGK equation. If, on the other hand, more than one collision occurs in every time step, most of the particle trajectory will consist of diffusive steps, and the scheme correspond to the diffusive approximation of the Boltzmann-BGK equation. The alternating kinetic and diffusive nature of a particle in the time domain is shown in Figure 1.

We will now briefly outline the details of the KD simulation scheme. We refer to [19] for more details on the KD scheme, and to [17] for more details on our particle model in the context of neutrals in a nuclear fusion reactor. Suppose a particle is released at time t_k with initial position $x(t_k) = x_k$ and Maxwellian post-collision velocity $v_k = \mu_v + \sigma_v \nu_k$, where ν_k is a standard normal random number. The particle then moves with this constant velocity until a collision occurs. If the collision rate is given by $R(x)$, the time τ_k until this collision is the solution of

$$\int_0^{\tau_k} R(x_k + v_k t) dt = \epsilon_k \quad (1)$$

where $\epsilon_k \sim \mathcal{E}(1)$ is an exponentially distributed random number. Equivalently, using a change of variables $x = x_k + v_k t$, τ_k is the solution of

$$\int_{x_k}^{x_k + v_k \tau_k} R(x) dx = \epsilon_k v_k. \quad (2)$$

In practice, and, also in our numerical experiments later on in Section 5, the collision rate is such that τ_k can easily be found from equation (1) or equation (2), e.g., $R(x)$ is a piecewise constant or piecewise linear function.

The particle thus collides at time $t_k + \tau_k$, at a position $x_k + v_k \tau_k$. In a standard kinetic simulation, the particle would now receive a new velocity from the Maxwellian post-collisional velocity distribution $v_{k+1} = \mu_v + \sigma_v \nu_{k+1}$, where ν_{k+1} is again a standard normal random number. The particle would then continue with this velocity until the next collision occurs. In the KD scheme, however, this new velocity v_{k+1} is only applied after the particle moves diffusively for the remainder of the current time interval. If

the time intervals have an equal length δt , this remaining time is

$$\theta_k = \delta t - (t_k + \tau_k \bmod \delta t). \quad (3)$$

The diffusive update during this time period θ_k is such that the mean and variance of the random walk correspond exactly to the mean and variance of the actual kinetic process, conditioned such that the final velocity is v_{k+1} . In [19], it is shown that this is the case if the advection coefficient in the random walk is chosen as

$$a_k = \mu_v \theta_k + (v_{k+1} - \mu_v) \frac{1}{R_k} (1 - e^{-R_k \theta_k}), \quad (4)$$

and if the diffusion coefficient is chosen as

$$d_k = \sqrt{\frac{2\sigma_v^2}{R_k^2} (2(e^{-R_k \theta_k} - 1) + R_k \theta_k (e^{-R_k \theta_k} + 1)) + \frac{(v_{k+1} - \mu_v)^2}{R_k^2} (1 - 2R_k \theta_k e^{-R_k \theta_k} - e^{-2R_k \theta_k})}, \quad (5)$$

and where we assumed the collision rate $R(x) = R_k$ remains constant within the time interval. In case R varies strongly with x within the time interval, some adaptations are required to equations (4) and (5), see [18]. These adaptations are applied in our numerical experiments in Section 5 later on.

In a single KD step, the particle thus moves to a time

$$t_{k+1} = t_k + \tau_k + \theta_k, \quad (6)$$

and a position

$$x_{k+1} = x_k + v_k \tau_k + a_k + d_k \chi_k, \quad (7)$$

where $\chi_k \sim \mathcal{N}(0, 1)$ is a standard normal random number. Remark that t_{k+1} is, by construction, a multiple of the time step δt . The process is then repeated with the next collision of the particle with velocity v_{k+1} . A complete algorithm for a KD simulation is shown in Algorithm 1. The main procedure, `KineticDiffusion`, consists of a repeated call to the subroutine `KineticDiffusionStep`, where the latter implements a single KD step, as outlined above. The procedure returns x_k , the position of the particle at time T after k KD steps, approximated with a time step δt .

3 Correlating fine and coarse particle paths

A key component in the MLMC method is the ability to generate correlated samples for particle trajectories with different time step sizes. These correlated sample paths must be chosen such that they approximate the same underlying continuous particle trajectory, so that the difference between the simulated particle paths follows mainly from the difference in time step size. Below, we will present a new and improved particle trajectory correlation scheme, which is one of the main contributions of this paper.

Let us introduce two time step sizes δt_ℓ and $\delta t_{\ell-1}$, with ℓ the “level” of approximation. A particle trajectory with time step size δt_ℓ thus corresponds to an approximation for the continuous particle trajectory with a relatively small time step size. This will be referred to as the *fine* particle trajectory. Similarly, a particle trajectory with time step size $\delta t_{\ell-1}$ corresponds to an approximation for the continuous particle trajectory with a relatively large time step size, and the trajectory will be referred to as the *coarse* particle trajectory. We will add this level parameters ℓ and $\ell - 1$ to all variables. For example, the initial position and velocity of the particle in the k th KD step with level ℓ are denoted by $x_{\ell,k}$ and $v_{\ell,k}$, respectively.

Algorithm 1: KD algorithm

input: simulation end time T , time step δt
output: position x_k of the particle at the end time T

```

1: procedure KineticDiffusion( $T, \delta t$ )                                     // main KD routine
2:    $k \leftarrow 0$ 
3:   sample  $\nu_k \sim \mathcal{N}(0, 1)$  and  $\epsilon_k \sim \mathcal{E}(1)$ 
4:   set  $x_k \leftarrow 1$ ,  $v_k \leftarrow \mu_v + \sigma_v \nu_k$  and  $t_k \leftarrow 0$            // initialize position, velocity & time
5:   solve equation (1) for  $\tau_k$  using  $\epsilon_k$                                            // compute time to first collision
6:   while  $t_k + \tau_k < T$  do                                                     // next collision is before end time  $T$ 
7:     sample  $\nu_{k+1} \sim \mathcal{N}(0, 1)$ ,  $\epsilon_{k+1} \sim \mathcal{E}(1)$  and  $\chi_k \sim \mathcal{N}(0, 1)$ 
8:      $x_{k+1}, v_{k+1}, t_{k+1}, \tau_{k+1}, \theta_k \leftarrow \text{KineticDiffusionStep}(x_k, v_k, t_k, \tau_k, \nu_{k+1}, \epsilon_{k+1}, \chi_k)$ 
9:      $k \leftarrow k + 1$ 
10:  end while
11:  if  $t_k < T$  then                                                             // move kinetically until end time  $T$ 
12:     $x_k \leftarrow x_k + v_k(T - t_k)$ 
13:  end if
14: end procedure

input: position  $x_k$ , velocity  $v_k$  and current time  $t_k$  of the particle,
        time  $\tau_k$  until the next kinetic event,
        random numbers  $\nu_{k+1}$ ,  $\epsilon_{k+1}$  and  $\chi_k$ 
output: new position  $x_{k+1}$ , new velocity  $v_{k+1}$  and new current time  $t_{k+1}$  of the particle,
        time  $\tau_{k+1}$  until the next kinetic event, duration  $\theta_k$  of previous diffusive step

15: procedure KineticDiffusionStep( $x_k, v_k, t_k, \tau_k, \nu_{k+1}, \epsilon_{k+1}, \chi_k$ )       // KD subroutine
16:    $v_{k+1} \leftarrow \mu_v + \sigma_v \nu_{k+1}$                                      // new particle velocity in next kinetic step
17:    $\theta_k \leftarrow \delta t - (\tau_k \bmod \delta t)$                              // duration of diffusive step (equation (3))
18:   compute  $a_k$  using (4) and  $d_k$  using (5)
19:    $x_{k+1} \leftarrow x_k + v_k \tau_k + (a_k + d_k \chi_k)$                          // update of the particle position (equation (7))
20:    $t_{k+1} \leftarrow t_k + \tau_k + \theta_k$                                        // update of the particle time (equation (6))
21:   solve equation (1) for  $\tau_{k+1}$  using  $\epsilon_{k+1}$                                // duration of next kinetic step
22: end procedure

```

A good correlation between a fine sample particle trajectory at level ℓ and a coarse sample particle trajectory at level $\ell - 1$ can be achieved by reusing the random numbers $\mathbf{y}_\ell := \{\nu_{\ell,k}, \epsilon_{\ell,k}, \chi_{\ell,k}\}_{k=0}^{K_\ell}$ from the simulation of the fine particle trajectory in the simulation of the coarse particle trajectory. To this end, let us define the operator $\varphi_\ell^{\ell-1} : \mathbf{y}_\ell \mapsto \tilde{\mathbf{y}}_{\ell,j}$, which maps the random numbers \mathbf{y}_ℓ to a set of random numbers $\tilde{\mathbf{y}}_{\ell-1} := \{\tilde{\nu}_{\ell-1,k}, \tilde{\epsilon}_{\ell-1,k}, \tilde{\chi}_{\ell-1,k}\}_{k=0}^{K_{\ell-1}}$ for the simulation of the coarse particle trajectory. Applying the operator $\varphi_\ell^{\ell-1}$ consists of two phases. First, the random numbers on level ℓ are mapped to the corresponding random numbers $\ell - 1$. Since the coarse particle trajectory corresponds to a simulation with a larger time step size, we expect $K_\ell > K_{\ell-1}$, and hence more than one random number used for the fine particle trajectory must be mapped to a single random number from the coarse particle trajectory, see Figure 2. After this *mapping* phase, the multiple random numbers from the fine particle trajectory must be aggregated into a single random number for the coarse particle trajectory. This is called the *aggregation* phase. We will discuss these two phases in turn in the remainder of this section.

3.1 Mapping the random numbers from the fine to the coarse particle path

Our mapping scheme can be summarized as follows. Let κ_k be the index of the next unused kinetic phase of the fine particle trajectory after $k - 1$ KD steps in the coarse particle path. The kinetic phase of the k th KD step in the coarse particle trajectory then uses the random numbers ν_{ℓ, κ_k} and $\epsilon_{\ell, \kappa_k}$, i.e.,

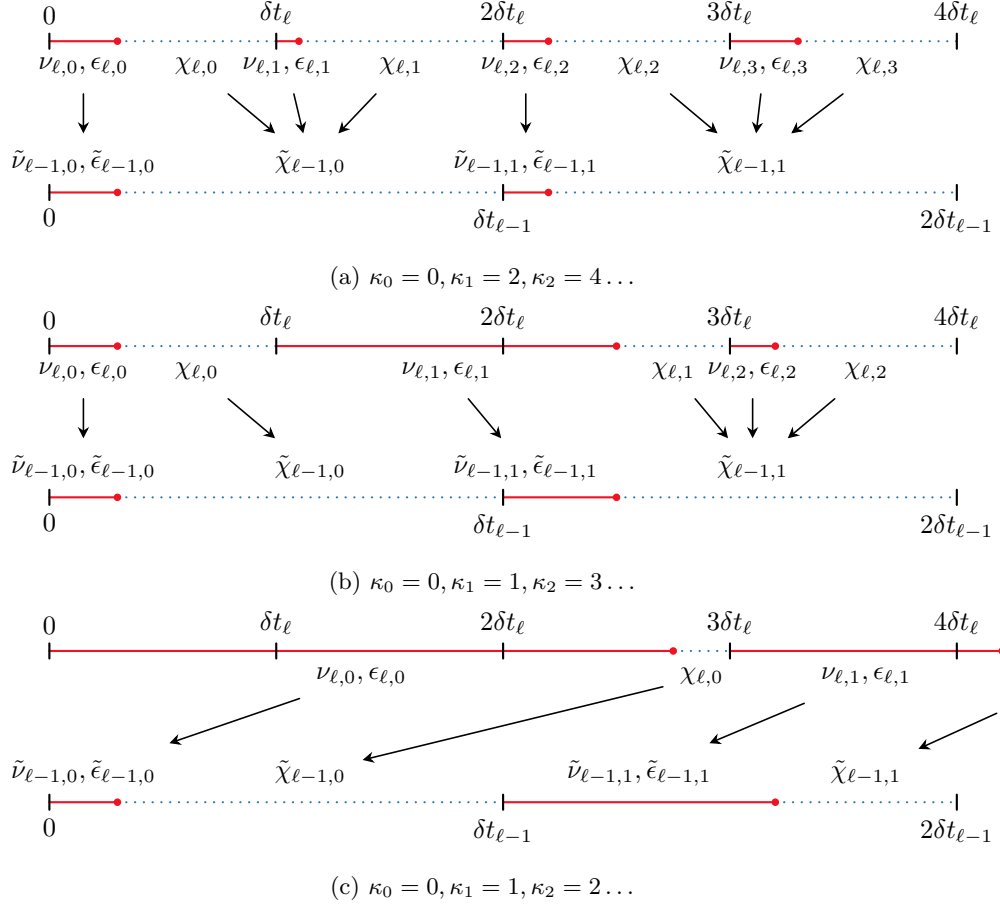


Figure 2: Examples of the mapping of the random numbers from the fine to the coarse particle path.

the random numbers of the κ_k th kinetic phase of the fine particle trajectory. The diffusive part of the k th KD step in the coarse particle trajectory uses an aggregation of all the random numbers $\nu_{\ell,m}$ and $\epsilon_{\ell,m}$, $m = \kappa_k + 1, \dots, \kappa_{k+1} - 1$, and $\chi_{\ell,m}$, $m = \kappa_k, \dots, \kappa_{k+1} - 1$, of the fine particle trajectory up to but not including the beginning of the first kinetic phase that extends beyond the end of the next coarse time step $\delta t_{\ell-1}$.

We refer to Figure 2 for an illustration of this mapping phase. Figure 2(a) shows the default case where, on average, there is one collision in every time step of the fine particle trajectory. In this case, the kinetic phase of the coarse particle path uses the random numbers from the corresponding kinetic phase of the fine particle path, and the diffusive phase of the coarse particle path uses one diffusive, one kinetic and again one diffusive phase of the fine particle path. Figure 2(b) shows a case where, on average, there is less than one collision event in every time step of the fine particle trajectory. In this case, we will only use the random numbers from the diffusive phase of the fine particle path for the diffusive phase of the coarse particle path. The length of the next kinetic phase of the coarse particle path, determined by $\epsilon_{\ell,2}$, will be adapted to reestablish the correlation, see the discussion of the aggregation phase in Section 3.2. Finally, Figure 2(c) shows a dramatic event that can occur only if the fine and coarse particle trajectories are already strongly decorrelated and both particles are in a part of the domain with a very different collision rate. We did not observe such a strong decorrelation in our numerical results in Section 5.

3.2 Aggregating the random numbers in the coarse path

After the mapping phase, outlined in Section 3.1, we must now specify how the random numbers \mathbf{y}_ℓ from the fine particle trajectory must be aggregated to the random numbers $\tilde{\mathbf{y}}_{\ell-1}$ for the coarse particle trajectory. The aggregation of the kinetic phase is straightforward. In the k th kinetic phase of the coarse particle trajectory, the random variable for the new Maxwellian post-collisional velocity is simply set to

$$\tilde{\nu}_{\ell-1,k} := \nu_{\ell,\kappa_k}, \quad (8)$$

where we recall the notation κ_k for the index of the next unused kinetic phase of the fine particle trajectory after $k-1$ KD steps in the coarse particle path. The length of the kinetic path is determined by

$$\tilde{\epsilon}_{\ell-1,k} := \epsilon_{\ell,\kappa_k} - \int_0^{t_{\ell-1,k} - t_{\ell,\kappa_k}} R(x_{\ell,\kappa_k} + v_{\ell,\kappa_k} t) dt, \quad (9)$$

see Figure 2(b). Because of the memorylessness of the exponential distribution, the random variable $\tilde{\epsilon}_{\ell-1,k}$ still follows the required (exponential) distribution.

In the k th diffusive phase of the coarse particle trajectory, the random number aggregation for $\tilde{\chi}_{\ell-1,k}$ uses a weighted sum of the normally distributed numbers $\nu_{\ell,m}$, $m = \kappa_k + 1, \dots, \kappa_{k+1} - 1$, and $\chi_{\ell,m}$, $m = \kappa_k, \dots, \kappa_{k+1} - 1$. With a suitable normalization, we set

$$\tilde{\chi}_{\ell-1,k} := \frac{\beta_{\kappa_k} \chi_{\ell,\kappa_k} + \sum_{m=\kappa_k+1}^{\kappa_{k+1}-1} (\alpha_m \nu_{\ell,m} + \beta_m \chi_{\ell,m})}{\sqrt{\beta_{\kappa_k}^2 + \sum_{m=\kappa_k+1}^{\kappa_{k+1}-1} (\alpha_m^2 + \beta_m^2)}}, \quad (10)$$

where the weights α_m , $m = \kappa_k + 1, \dots, \kappa_{k+1} - 1$, and β_m , $m = \kappa_k, \dots, \kappa_{k+1} - 1$, not all zero, will be specified below.

Recall that the particle position can be computed as

$$x_{\ell,K_\ell} = \underbrace{\tau_{\ell,0}(\mu_v + \sigma_v \nu_{\ell,0})}_{\text{kinetic}} + \underbrace{a_{\ell,0} + d_{\ell,0} \chi_{\ell,0}}_{\text{diffusion}} + \underbrace{\tau_{\ell,1}(\mu_v + \sigma_v \nu_{\ell,1})}_{\text{kinetic}} + \underbrace{a_{\ell,1} + d_{\ell,1} \chi_{\ell,1}}_{\text{diffusion}} + \dots,$$

where $\tau_{\ell,k}$ is determined by $\epsilon_{\ell,k}$, and where $a_{\ell,k}$ and $d_{\ell,k}$ depend on $\epsilon_{\ell,k}$ and $\nu_{\ell,k+1}$. In effect, this means that the random variable $\nu_{\ell,k+1}$ plays a role for a longer time than just the duration of the kinetic phase $\tau_{\ell,k+1}$, and this excess time appears in the duration of the previous diffusive phase $\theta_{\ell,k}$. To incorporate this aspect of dependence between different time steps in our aggregation scheme, we transfer the expected time during which $\nu_{\ell,k+1}$ plays a role in the diffusive phase to the next kinetic phase. This time, which we will denote by $\zeta_{\ell,m}$, is equal to the expected time of the diffusive phase in which the final velocity is used, i.e.,

$$\zeta_{\ell,m} := \frac{1}{R_m} (1 - e^{-R_m \theta_{\ell,m}}).$$

The duration of the kinetic and diffusive phase are thus updated to

$$\tau'_{\ell,m+1} := \tau_{\ell,m+1} + \zeta_{\ell,m}, \quad \text{respectively} \quad \theta'_{\ell,m} := \theta_{\ell,m} - \zeta_{\ell,m}.$$

The weights α_m , $m = \kappa_k + 1, \dots, \kappa_{k+1} - 1$, for the normally distributed random numbers $\nu_{\ell,m}$, are chosen

as the modified kinetic time, during which the velocity $\nu_{\ell,m}$ determines the kinetic motion, i.e.,

$$\alpha_m := \tau'_{\ell,m} \sigma_v.$$

The weights β_m , $m = \kappa_k, \dots, \kappa_{k+1} - 1$, for the normally distributed random numbers $\chi_{\ell,m}$, are chosen as

$$\beta_m := \sqrt{\frac{2\sigma_v^2}{R_m^2} \left(e^{-R_m \theta'_{\ell,m}} + R_m \theta'_{\ell,m} - 1 \right)}.$$

These weights are equal to the standard deviation of the diffusive position update without conditioning on the final velocity $v_{\ell,m+1}$.

3.3 An algorithm for correlated KD sampling

A complete algorithm for correlated KD sampling is shown in Algorithm 2. The routine `CorrelatedKineticDiffusion` moves the particle simultaneously on the coarse and fine particle trajectory in one sweep over the time domain. The procedure reuses the subroutine `KineticDiffusionStep` from Algorithm 1. The output of the procedure is x_{ℓ,k_1} and $x_{\ell-1,k_2}$, two correlated samples of the particle positions at time T , approximated with a time step δt_ℓ , respectively $\delta t_{\ell-1}$.

Algorithm 2: Correlated KD algorithm

input: simulation end time T , time steps δt_ℓ and $\delta t_{\ell-1}$

output: positions x_{ℓ,k_1} and $x_{\ell-1,k_2}$ of the particle at the end time T

```

1: procedure CorrelatedKineticDiffusion( $T, \delta t_\ell, \delta t_{\ell-1}$ )
2:   set  $k_1 \leftarrow 0$  and  $k_2 \leftarrow 0$ 
3:   sample  $\nu_{\ell,k_1} \sim \mathcal{N}(0, 1)$  and  $\epsilon_{\ell,k_1} \sim \mathcal{E}(1)$ 
4:   set  $\tilde{\nu}_{\ell-1,k_2} \leftarrow \nu_{\ell,k_1}$  and  $\tilde{\epsilon}_{\ell-1,k_2} \leftarrow \epsilon_{\ell,k_1}$ 
5:   set  $x_{\ell,k_1} \leftarrow 1$ ,  $v_{\ell,k_1} \leftarrow \mu_v + \sigma_v \nu_{\ell,k_1}$  and  $t_{\ell,k_1} \leftarrow 0$  // initialize position, velocity & time
6:   set  $x_{\ell-1,k_2} \leftarrow 1$ ,  $v_{\ell-1,k_2} \leftarrow \mu_v + \sigma_v \tilde{\nu}_{\ell-1,k_2}$  and  $t_{\ell-1,k_2} \leftarrow 0$  // ... same for coarse path
7:   solve equation (1) for  $\tau_{\ell,k_1}$  and set  $\tau_{\ell-1,k_2} \leftarrow \tau_{\ell,k_1}$  // compute time to first collision
8:   while  $t_{\ell-1} + \tau_{\ell-1} < T$  do // next coarse collision is before end time  $T$ 
9:     /* repeat until next random number aggregation from fine to coarse path */
10:    repeat // move the fine particle path
11:      sample  $\nu_{\ell,k_1+1} \sim \mathcal{N}(0, 1)$ ,  $\epsilon_{\ell,k_1+1} \sim \mathcal{E}(1)$  and  $\chi_{\ell,k_1} \sim \mathcal{N}(0, 1)$ 
12:       $x_{\ell,k_1+1}, v_{\ell,k_1+1}, t_{\ell,k_1+1}, \tau_{\ell,k_1+1}, \theta_{\ell,k_1} \leftarrow$ 
13:        KineticDiffusionStep( $x_{\ell,k_1}, v_{\ell,k_1}, t_{\ell,k_1}, \tau_{\ell,k_1}, \nu_{\ell,k_1+1}, \epsilon_{\ell,k_1+1}, \chi_{\ell,k_1}$ )
14:       $k_1 \leftarrow k_1 + 1$ 
15:    until  $\lceil (t_{\ell,k_1} + \tau_{\ell,k_1}) / \delta t_\ell \rceil \delta t_\ell > \lceil (t_{\ell-1,k_2} + \tau_{\ell-1,k_2}) / \delta t_{\ell-1} \rceil \delta t_{\ell-1}$ 
16:    set  $\tilde{\nu}_{\ell-1,k_2+1} \leftarrow \nu_{\ell,k_1}$  // equation (8)
17:    compute  $\tilde{\epsilon}_{\ell-1,k_2+1}$  according to equation (9) and  $\tilde{\chi}_{\ell-1,k_2}$  according to equation (10)
18:     $x_{\ell-1,k_2+1}, v_{\ell-1,k_2+1}, t_{\ell-1,k_2+1}, \tau_{\ell-1,k_2+1}, \theta_{\ell-1,m} \leftarrow$ 
19:      KineticDiffusionStep( $x_{\ell-1,k_2}, v_{\ell-1,k_2}, t_{\ell-1,k_2}, \tau_{\ell-1,k_2}, \tilde{\nu}_{\ell-1,k_2+1}, \tilde{\epsilon}_{\ell-1,k_2+1}, \tilde{\chi}_{\ell-1,k_2}$ )
20:     $k_2 \leftarrow k_2 + 1$ 
21:  end while
22:  if  $t_{\ell,k_1} + \tau_{\ell,k_1} < T$  then // move fine particle path kinetically until time  $T$ 
23:     $x_{\ell,k_1} \leftarrow x_{\ell,k_1} + v_{\ell,k_1} (T - \tau_{\ell,k_1})$ 
24:  end if
25:  if  $t_{\ell-1,k_2} + \tau_{\ell-1,k_2} < T$  then // move coarse particle path kinetically until time  $T$ 
26:     $x_{\ell-1,k_2} \leftarrow x_{\ell-1,k_2} + v_{\ell-1,k_2} (T - \tau_{\ell-1,k_2})$ 
27:  end if
28: end procedure

```

4 Multilevel Asymptotic-Preserving Monte Carlo

In this section, we outline the details of our ML-APMC method. First, in Section 4.1, we briefly discuss the MLMC method. This multilevel method uses a hierarchy of coarser approximations with ever larger time step sizes, to reduce the cost of the MC simulation. Next, in Section 4.2, we discuss the specific challenges in applying the MLMC method to the APMC scheme from Section 2. Notably, the behavior of variance and cost of the multilevel differences with increasing level parameter ℓ is not the usual monotone behavior as observed in models described by differential equations, see [5, 12]. This atypical behavior poses challenges for the level selection problem, i.e., the choice of the coarser time step sizes that are included in the multilevel hierarchy.

4.1 Multilevel sampling

Let us introduce the set of time step sizes $\{\delta t_\ell := T/2^\ell\}_{\ell=0}^L$. These time step sizes discretize the time domain $[0, T]$ into 2^ℓ time intervals $[i \cdot \delta t_\ell, (i+1) \cdot \delta t_\ell]$ for $i = 0, 1, \dots, 2^\ell - 1$. Furthermore, let $x_\ell(t, \mathbf{y}_\ell)$ denote the position of a particle at time t , computed using a time step $\delta t_\ell = T/2^\ell$, where T is the end time and $\ell \geq 0$ is the level of approximation. Here, we explicitly denote the dependence of the particle position x_ℓ on the random variables $\mathbf{y}_\ell = \{\nu_{\ell,k}, \epsilon_{\ell,k}, \chi_{\ell,k}\}_{k=0}^{K_\ell}$ used to simulate the trajectory of the particle. Our goal is to compute the position of the particle at the end time T , i.e., $x_\ell(T, \mathbf{y}_\ell)$. This position is the *quantity of interest*, hereafter denoted as

$$Q_\ell(\mathbf{y}_\ell) := x_\ell(T, \mathbf{y}_\ell).$$

Sometimes, the argument will be dropped when the meaning is clear from the context, i.e., we write Q_ℓ instead of $Q_\ell(\mathbf{y}_\ell)$. The n th i.i.d. sample of this random variable Q_ℓ is denoted as

$$Q_\ell(\mathbf{y}_\ell^{(n)}) := x_\ell(T, \mathbf{y}_\ell^{(n)}) \text{ with } \mathbf{y}_\ell^{(n)} := \{\nu_{\ell,k}^{(n)}, \epsilon_{\ell,k}^{(n)}, \chi_{\ell,k}^{(n)}\}_{k=0}^{K_\ell^{(n)}}.$$

Furthermore, let $\{0, 1, \dots, L\}$ be the set of all possible levels, in increasing order, and let $\mathcal{L} \subseteq \{0, 1, \dots, L\}$ be an ordered subset of levels of length J , with $0 < J \leq L+1$, defined as $\mathcal{L} := \{\ell_j\}_{j=1}^J$ where $0 \leq \ell_1 < \dots < \ell_J = L$. Note that we restrict our attention to subsets that include the level with highest accuracy L , i.e., $\ell_J = L$. If $J = 1$, then $\mathcal{L} = \{L\}$, and only the most accurate level $\ell_J = L$ is used. On the other hand, if $J = L+1$, then all levels $0, 1, 2, \dots, L$ are included in the set \mathcal{L} . The set of all feasible subsets \mathcal{L} will be denoted by $\mathcal{S}_\mathcal{L}$.

The MLMC estimator for the expected value of the quantity of interest on level L is

$$\mathcal{Q}_\mathcal{L} := \frac{1}{N_{\ell_1}} \sum_{n=1}^{N_{\ell_1}} Q_{\ell_1}(\mathbf{y}_{\ell_1}^{(n)}) + \sum_{j=2}^J \frac{1}{N_{\ell_j}} \sum_{n=1}^{N_{\ell_j}} \left(Q_{\ell_j}(\mathbf{y}_{\ell_j}^{(n)}) - Q_{\ell_{j-1}}(\tilde{\mathbf{y}}_{\ell_{j-1}}^{(n)}) \right),$$

where all $\mathbf{y}_{\ell_j}^{(n)}$ are i.i.d. samples for each $n = 1, 2, \dots, N_{\ell_j}$ and for each $\ell_j \in \mathcal{L}$, and with N_{ℓ_j} the total number of samples on level ℓ_j . The random variables $\tilde{\mathbf{y}}_{\ell_{j-1}}^{(n)}$ are defined as

$$\tilde{\mathbf{y}}_{\ell_{j-1}}^{(n)} := \{\tilde{\nu}_{\ell_{j-1},k}^{(n)}, \tilde{\epsilon}_{\ell_{j-1},k}^{(n)}, \tilde{\chi}_{\ell_{j-1},k}^{(n)}\}_{k=0}^{\tilde{K}_{\ell_{j-1}}^{(n)}},$$

where $\tilde{\nu}_{\ell_{j-1},k}^{(n)}$, $\tilde{\epsilon}_{\ell_{j-1},k}^{(n)}$ and $\tilde{\chi}_{\ell_{j-1},k}^{(n)}$ are computed using the mapping and aggregation $\varphi_{\ell_j}^{\ell_{j-1}} : \mathbf{y}_{\ell_j}^{(n)} \mapsto \tilde{\mathbf{y}}_{\ell_{j-1}}^{(n)}$ from Section 3.2 applied to $\mathbf{y}_{\ell_j}^{(n)}$, for each $k = 0, 1, \dots, \tilde{K}_{\ell_{j-1}}^{(n)}$, and with $\tilde{K}_{\ell_{j-1}}^{(n)}$ the number of collisions in the n th coarse aggregated particle path.

Using the shorthand notation $\Delta Q_{\ell_i, \ell_j} := Q_{\ell_i}(\mathbf{y}_{\ell_i}) - Q_{\ell_j}(\tilde{\mathbf{y}}_{\ell_j})$ for a multilevel *difference*, the MLMC estimator can be written compactly as

$$\mathcal{Q}_{\mathcal{L}} = \frac{1}{N_{\ell_1}} \sum_{n=1}^{N_{\ell_1}} Q_{\ell_1}^{(n)} + \sum_{j=2}^J \frac{1}{N_{\ell_j}} \sum_{n=1}^{N_{\ell_j}} \Delta Q_{\ell_j, \ell_{j-1}}^{(n)}, \quad (11)$$

where $\Delta Q_{\ell_j, \ell_{j-1}}^{(n)} := Q_{\ell_j}(\mathbf{y}_{\ell_j}^{(n)}) - Q_{\ell_{j-1}}(\tilde{\mathbf{y}}_{\ell_{j-1}}^{(n)})$ denotes the n th realization of $\Delta Q_{\ell_j, \ell_{j-1}}$, and $Q_{\ell_1}^{(n)} := Q_{\ell_1}(\mathbf{y}_{\ell_1}^{(n)})$. For later use, let us also define $E_{\ell_i} := |\mathbb{E}[Q_{\ell_i}]|$, $E_{\ell_i, \ell_j} := |\mathbb{E}[\Delta Q_{\ell_i, \ell_j}]|$, $V_{\ell_i} := \mathbb{V}[Q_{\ell_i}]$, $V_{\ell_i, \ell_j} := \mathbb{V}[\Delta Q_{\ell_i, \ell_j}]$, $C_{\ell_i} := \mathcal{C}(Q_{\ell_i})$ and $C_{\ell_i, \ell_j} := \mathcal{C}(Q_{\ell_i}) + \mathcal{C}(Q_{\ell_j})$, where $\mathcal{C}(Z)$ denotes the cost of computing a single realization of the random variable Z .

It is easy to see that the multilevel estimator is an unbiased estimator for $\mathbb{E}[Q_L]$, since

$$\begin{aligned} \mathbb{E}[\mathcal{Q}_{\mathcal{L}}] &= \mathbb{E}[Q_{\ell_1}(\mathbf{y}_{\ell_1})] + \sum_{j=2}^J \mathbb{E}[Q_{\ell_j}(\mathbf{y}_{\ell_j}) - Q_{\ell_{j-1}}(\tilde{\mathbf{y}}_{\ell_{j-1}})] \\ &= \mathbb{E}[Q_{\ell_1}(\mathbf{y}_{\ell_1})] + \mathbb{E}[Q_{\ell_2}(\mathbf{y}_{\ell_2}) - Q_{\ell_1}(\tilde{\mathbf{y}}_{\ell_1})] + \dots + \mathbb{E}[Q_{\ell_J}(\mathbf{y}_{\ell_J}) - Q_{\ell_{J-1}}(\tilde{\mathbf{y}}_{\ell_{J-1}})] \end{aligned} \quad (12)$$

$$= \mathbb{E}[Q_{\ell_J}(\mathbf{y}_{\ell_J})] = \mathbb{E}[Q_L], \quad (13)$$

where we used the linearity of the $\mathbb{E}[\cdot]$ -operator and the fact that the random variables \mathbf{y}_{ℓ_j} and $\tilde{\mathbf{y}}_{\ell_{j-1}}$ have the same distribution. We will verify this assumption later on in the numerical experiments in Section 5.1. Note that equation (13) is the motivation for our earlier restriction that $\ell_J = L$. By including the level L with highest accuracy into the set \mathcal{L} , the multilevel estimator is unbiased estimator for the expected value of the quantity of interest on that level. The variance of the multilevel estimator can be expressed as

$$\mathbb{V}[\mathcal{Q}_{\mathcal{L}}] = \frac{\mathbb{V}[Q_{\ell_1}(\mathbf{y}_{\ell_1})]}{N_{\ell_1}} + \sum_{j=2}^J \frac{\mathbb{V}[Q_{\ell_j}(\mathbf{y}_{\ell_j}) - Q_{\ell_{j-1}}(\tilde{\mathbf{y}}_{\ell_{j-1}})]}{N_{\ell_j}} = \frac{V_{\ell_1}}{N_{\ell_1}} + \sum_{j=2}^J \frac{V_{\ell_j, \ell_{j-1}}}{N_{\ell_j}},$$

where we again used the observation that the random variables \mathbf{y}_{ℓ_j} and $\tilde{\mathbf{y}}_{\ell_{j-1}}$ have the same distribution, and that \mathbf{y}_{ℓ_j} and \mathbf{y}_{ℓ_k} are independent for any $j \neq k$.

There are two sources of error in the MLMC estimator in equation (11): the discretization error, related to the finite time step δt_L , and the stochastic error, present because we replace the expected value by a sample average of a finite set of samples. The accuracy of the estimator can be quantified using the mean square error (MSE), where these two sources of error become apparent:

$$\begin{aligned} \text{MSE}(\mathcal{Q}_{\mathcal{L}}) &:= \mathbb{E}[(\mathcal{Q}_{\mathcal{L}} - \mathbb{E}[Q])^2] \\ &= \mathbb{E}[(\mathcal{Q}_{\mathcal{L}} - \mathbb{E}[\mathcal{Q}_{\mathcal{L}}])^2] + (\mathbb{E}[\mathcal{Q}_{\mathcal{L}}] - \mathbb{E}[Q])^2 \\ &= \underbrace{\left(\frac{V_{\ell_1}}{N_{\ell_1}} + \sum_{j=2}^J \frac{V_{\ell_j, \ell_{j-1}}}{N_{\ell_j}} \right)}_{\text{variance}} + \underbrace{(\mathbb{E}[Q_L - Q])^2}_{\text{bias}} \end{aligned} \quad (14)$$

The first term in equation (14) is the variance of the estimator, representing the stochastic part of the error. The second term in equation (14) is the square of the bias of the estimator, representing the discretization error. To impose an MSE of at most ε^2 , or, equivalently, a *root mean square error* (RMSE)

of at most ε , it is now sufficient to enforce that

$$\frac{V_{\ell_1}}{N_{\ell_1}} + \sum_{j=2}^J \frac{V_{\ell_j, \ell_{j-1}}}{N_{\ell_j}} \leq \frac{\varepsilon^2}{2} \quad (\text{statistical constraint}), \text{ and} \quad (15)$$

$$|\mathbb{E}[Q_L - Q]| \leq \frac{\varepsilon}{\sqrt{2}} \quad (\text{bias constraint}). \quad (16)$$

Two unknowns remain in the formulation of the MLMC estimator in equation (11).

- The **number of samples** N_{ℓ_j} , for each $j = 1, 2, \dots, J$. This number of samples can be found by minimizing the total cost of the estimator, while ensuring that the statistical constraint, i.e., equation (15), is satisfied.
- The **choice of levels** $\mathcal{L} = \{\ell_j\}_{j=1}^J$. The optimal set of levels can be found by minimizing the total cost of the estimator, while ensuring that the bias constraint, i.e., equation (16), is satisfied.

We will address the first problem, i.e., determining the optimal set of levels $\{N_{\ell_j}\}_{j=1}^J$, in the remainder of this section. The second problem, i.e., the level selection strategy, will be tackled in the next section.

The total cost of the MLMC estimator can be expressed as

$$\mathcal{C}(\mathcal{Q}_{\mathcal{L}}) = N_{\ell_1} C_{\ell_1} + \sum_{j=2}^J N_{\ell_j} C_{\ell_j, \ell_{j-1}}.$$

Next, consider the constrained minimization problem

$$\begin{aligned} \min_{N_{\ell_1}, N_{\ell_2}, \dots, N_{\ell_J}} \quad & N_{\ell_1} C_{\ell_1} + \sum_{j=2}^J N_{\ell_j} C_{\ell_j, \ell_{j-1}} \\ \text{s.t.} \quad & \frac{V_{\ell_1}}{N_{\ell_1}} + \sum_{j=2}^J \frac{V_{\ell_j, \ell_{j-1}}}{N_{\ell_j}} = \frac{\varepsilon^2}{2}, \end{aligned}$$

see, e.g., [12] for details. The Lagrangian of this problem is

$$\mathcal{L}(N_{\ell_1}, N_{\ell_2}, \dots, N_{\ell_J}) = N_{\ell_1} C_{\ell_1} + \sum_{j=2}^J N_{\ell_j} C_{\ell_j, \ell_{j-1}} + \zeta \left(\frac{V_{\ell_1}}{N_{\ell_1}} + \sum_{j=2}^J \frac{V_{\ell_j, \ell_{j-1}}}{N_{\ell_j}} - \frac{\varepsilon^2}{2} \right),$$

where ζ is a Lagrange multiplier and where we treat the unknowns $N_{\ell_1}, N_{\ell_2}, \dots, N_{\ell_J}$ as continuous variables. Proceeding as usual, the first-order necessary optimality conditions are

$$\begin{cases} \frac{\partial \mathcal{L}}{\partial N_{\ell_1}} = C_{\ell_1} - \zeta \frac{V_{\ell_1}}{N_{\ell_1}^2} = 0, \\ \frac{\partial \mathcal{L}}{\partial N_{\ell_j}} = C_{\ell_j, \ell_{j-1}} - \zeta \frac{V_{\ell_j, \ell_{j-1}}}{N_{\ell_j}^2} = 0 \quad \text{for each } j = 2, 3, \dots, J, \text{ and} \\ \frac{\partial \mathcal{L}}{\partial \zeta} = \frac{V_{\ell_1}}{N_{\ell_1}} + \sum_{j=2}^J \frac{V_{\ell_j, \ell_{j-1}}}{N_{\ell_j}} - \frac{\varepsilon^2}{2} = 0. \end{cases}$$

The solution of this system of equations is

$$\begin{aligned} N_{\ell_1} &= \frac{2}{\varepsilon^2} \sqrt{\frac{V_{\ell_1}}{C_{\ell_1}}} \left(\sqrt{V_{\ell_1} C_{\ell_1}} + \sum_{j=2}^J \sqrt{V_{\ell_j, \ell_{j-1}} C_{\ell_j, \ell_{j-1}}} \right), \text{ and} \\ N_{\ell_j} &= \frac{2}{\varepsilon^2} \sqrt{\frac{V_{\ell_j, \ell_{j-1}}}{C_{\ell_j, \ell_{j-1}}}} \left(\sqrt{V_{\ell_1} C_{\ell_1}} + \sum_{j=2}^J \sqrt{V_{\ell_j, \ell_{j-1}} C_{\ell_j, \ell_{j-1}}} \right) \text{ for } j = 2, 3, \dots, J. \end{aligned} \quad (17)$$

In an actual implementation of the ML-APMC estimator, these values can be rounded up to the nearest integer to enforce an integer number of samples, and sample variances and cost estimates can replace the quantities V_{ℓ_1} , $V_{\ell_j, \ell_{j-1}}$, C_{ℓ_1} and $C_{\ell_j, \ell_{j-1}}$.

Substituting the optimal values for N_{ℓ_1} , N_{ℓ_2} , \dots , N_{ℓ_J} from (17) into the total cost of the MLMC estimator, we find that

$$\mathcal{C}(\mathcal{Q}_{\mathcal{L}}) = \frac{2}{\varepsilon^2} \left(\sqrt{V_{\ell_1} C_{\ell_1}} + \sum_{j=2}^J \sqrt{V_{\ell_j, \ell_{j-1}} C_{\ell_j, \ell_{j-1}}} \right)^2. \quad (18)$$

We will use this expression for the total cost of the estimator in the next section, when computing the optimal selection of levels \mathcal{L} in Section 4.2 below.

We remark that, for the APMC scheme outlined in Section 2, the behavior of the variances $V_{\ell_j, \ell_{j-1}}$ and costs $C_{\ell_j, \ell_{j-1}}$ is highly nontrivial, and different from the usual monotone behavior in the case of SDEs, as shown in [12], or in the case of PDEs with random coefficients, as shown in, e.g., [5]. See Figure 8 and the discussion in Section 5.2 below for details. This nontrivial behavior poses an additional difficulty when selecting the level set \mathcal{L} below. Furthermore, the standard theoretical convergence results for MLMC, as presented in, e.g., [12], cannot be used in our case. However, our numerical results in Section 5 illustrate that our method achieves the usual cost complexity rate $\mathcal{O}(\varepsilon^{-2})$, where ε is the tolerance on the RMSE.

4.2 Level selection

In this section, we are looking for the subset of levels $\mathcal{L}^* \in S_{\mathcal{L}}$ that yields the MLMC estimator with smallest possible cost, while ensuring that the bias constraint, i.e., equation (16) is satisfied. The latter constraint can be satisfied by choosing a suitable most accurate level L . This value L will be larger for smaller tolerances ε^2 imposed on the MSE, i.e., equation (14). Since, by construction, any feasible subset \mathcal{L} contains the most accurate level L , we can assume constraint (16) is always satisfied.

Using the expression for the total cost of the MLMC estimator from equation (18), the optimal subset of levels \mathcal{L}^* is

$$\mathcal{L}^* = \arg \min_{\mathcal{L} \in S_{\mathcal{L}}} \left(\sqrt{V_{\ell_1} C_{\ell_1}} + \sum_{j=2}^J \sqrt{V_{\ell_j, \ell_{j-1}} C_{\ell_j, \ell_{j-1}}} \right). \quad (19)$$

Thus, \mathcal{L}^* is the solution of a combinatorial optimization problem. This problem could be solved using a brute-force approach, where we compute the value of the cost function for every feasible subset $\mathcal{L} \in S_{\mathcal{L}}$, for a given finest level L . However, this approach quickly becomes intractable, even for moderate values

of L . Accordingly, let us introduce the dummy variables

$$\begin{aligned} u_i &:= \begin{cases} 1 & \text{if } \ell_1 = i \\ 0 & \text{otherwise} \end{cases} & \text{for } i = 0, 1, \dots, L, \text{ and} \\ w_{i,j} &:= \begin{cases} 1 & \text{if } \ell_i \in \mathcal{L} \wedge \ell_j \in \mathcal{L} \\ 0 & \text{otherwise} \end{cases} & \text{for } i = 1, 2, \dots, L \text{ and } j = 0, 1, \dots, i-1. \end{aligned}$$

The unconstrained combinatorial optimization problem in equation (19) can be written as a constrained integer linear programming problem

$$\begin{aligned} \min_{u_i, w_{i,j}} & \left(\sum_{i=0}^L \left(u_i \sqrt{V_i C_i} \right) + \sum_{i=1}^L \sum_{j=0}^{i-1} \left(w_{i,j} \sqrt{V_{i,j} C_{i,j}} \right) \right), \\ \text{subject to } & u_i \in \{0, 1\} & i = 0, 1, \dots, L, \\ & w_{i,j} \in \{0, 1\} & i = 1, 2, \dots, L, \ j = 0, 1, \dots, i-1 \\ & \sum_{i=j+1}^L w_{i,j} \leq 1 & j = 0, 1, \dots, L-1, \\ & \sum_{j=0}^{i-1} w_{i,j} \leq 1 & i = 1, 2, \dots, L-1, \\ & \sum_{j=0}^{L-1} w_{L,j} = 1 \\ & \sum_{j=0}^{k-1} w_{k,j} - \sum_{i=k+1}^L w_{i,k} = 0 & k = 1, 2, \dots, L-1, \\ & \sum_{i=0}^L u_i = 1 & i = 0, 1, \dots, L. \end{aligned} \tag{20}$$

The optimal set of levels \mathcal{L}^* then simply consists of all levels i where $u_i = 1$ or $w_{i,j} = 1$. Dedicated methods exist for solving (20), including *branch-and-bound* methods, see, e.g., [1], and *cutting plane* methods, see, e.g., [21]. However, this approach suffers from a major drawback: it assumes that the $L(L-1)/2$ values for the variances $V_{i,j}$, $i = 1, 2, \dots, L$ and $j = 0, 1, \dots, i-1$, are available. To circumvent this problem, we use the following strategy. By definition, the variance $V_{i,j}$ can be expressed as

$$V_{i,j} = V_i + V_j - 2\rho_{i,j}\sqrt{V_i V_j},$$

where $\rho_{i,j}$ is the correlation between Q_i and Q_j . Comparing Q_i and Q_j with Q_L , we find that

$$\rho_{L,i}\rho_{L,j} - \sqrt{\rho_{L,i}^2\rho_{L,j}^2 + 1 - \rho_{L,i}^2 - \rho_{L,j}^2} \leq \rho_{i,j} \leq \rho_{L,i}\rho_{L,j} + \sqrt{\rho_{L,i}^2\rho_{L,j}^2 + 1 - \rho_{L,i}^2 - \rho_{L,j}^2},$$

where $\rho_{L,i}$ is the correlation coefficient between Q_L and Q_i , and $\rho_{L,j}$ is the correlation coefficient between Q_L and Q_j . Assuming that $\rho_{i,j}$ is the geometric mean of both extremes, we find that

$$\rho_{i,j}^2 + 1 \approx \rho_{L,i}^2 + \rho_{L,j}^2,$$

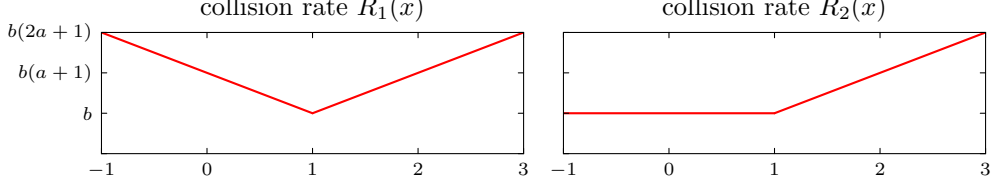


Figure 3: Collision rate $R_1(x)$ for the symmetric background B_1 (left) and collision rate $R_2(x)$ for the asymmetric background B_2 (right).

and hence

$$V_{i,j} \approx V_i + V_j - 2\sqrt{(\rho_{L,i}^2 + \rho_{L,j}^2 - 1)V_i V_j}.$$

The latter expression can be obtained from the $L+1$ values V_i , $i = 0, 1, \dots, L$ and the L values $\rho_{L,i}$, $i = 0, 1, \dots, L-1$. In our numerical experiments presented below, we use sample variances and sample correlation coefficients to approximate V_i and $\rho_{L,i}$, based on a pilot run with a limited number of samples on each level. From this set of samples, we can also extract actual run times that can replace the cost estimates C_i and $C_{i,j}$ in equation (20).

5 Numerical results

In this section, we apply our ML-APMC method to compute the expected value of the particle position for a one-dimensional fusion test-case inspired by [8]. We set up a simulation for $t \in [0, T]$ with end time $T = 1$. Particles are released from their initial position $x(0) = 1$, and collide with two different backgrounds $B_1 := \{R_1(x), \mu_v, \sigma_v\}$ and $B_2 := \{R_2(x), \mu_v, \sigma_v\}$ with $\mu_v = 0$, $\sigma_v = 1$ and collision rates

$$R_1(x) = \begin{cases} -b(a(x-1)-1) & x \leq 1 \\ b(a(x-1)+1) & x > 1 \end{cases} \quad \text{and} \quad R_2(x) = \begin{cases} b & x \leq 1 \\ b(a(x-1)+1) & x > 1 \end{cases}.$$

These collision rates are shown in Figure 3. For obvious reasons, we call B_1 a *symmetric* background, and B_2 an *asymmetric* background. We refer to the background with $a = 0$ as the *homogeneous* case, since, in that case, the collision rate is constant, i.e., we have $R_1(x) = R_2(x) = b$. A background with $a \gg 0$ is referred to as the *heterogeneous* case. We choose the background parameters as $a \in \{0, 0.1, 0.2, 0.5, 1, 2, 5, 10, 20, 50, 100\}$ and $b \in \{1, 10, 100, 1\,000, 10\,000, 100\,000\}$.

Our main numerical results are divided into three subsections. First, in Section 5.1, we will check the consistency of the random number mapping and aggregation $\varphi_{\ell_j}^{\ell_{j-1}} : \mathbf{y}_{\ell_j}^{(n)} \mapsto \tilde{\mathbf{y}}_{\ell_{j-1}}^{(n)}$ from Section 3 numerically. That is, we will verify if the aggregated random numbers $\tilde{\mathbf{y}}_{\ell_{j-1}}^{(n)}$ for the coarse particle path satisfy the required distributions. Next, in Section 5.2, we study the level selection strategy from Section 4.2, and devise a heuristic algorithm for level selection in the ML-APMC method. Finally, in Section 5.3, we compare the efficiency of the new ML-APMC scheme with the standard, single-level APMC scheme.

In all our numerical experiments below, we used our implementation of the APMC scheme, available online at <https://github.com/PieterjanRobbe/ML-APMC.jl>, and the MLMC code `MultilevelEstimators`, available online at <https://github.com/PieterjanRobbe/MultilevelEstimators.jl>.

5.1 Coarse particle path consistency

In this section, we numerically verify the consistency of the random numbers used for the coarse correlated particle path. That is, we will assert whether the random numbers $\tilde{\mathbf{y}}_{\ell_{j-1}}^{(n)}$, defined by the mapping $\varphi_{\ell_j}^{\ell_{j-1}}$ from Section 3, follow the required distributions. The Anderson–Darling (AD) hypothesis test can be used to test whether a given set of samples is drawn from a certain probability distribution. Let $\Phi(x)$ denote the cumulative distribution function (CDF) of the proposed distribution, and let $\Phi_N(x)$ denote the empirical CDF obtained from N samples $\{\xi^{(n)}\}_{n=1}^N$ of the random variable ξ . Recall that the latter is computed as

$$\Phi_N(x) := \frac{1}{N} \sum_{n=1}^N \mathbb{1}_{\xi^{(n)} \leq x},$$

where $\mathbb{1}_{\xi^{(n)} \leq x}$ is the indicator function for event $\xi^{(n)} \leq x$. The AD test computes the metric

$$A^2 = N \int_{-\infty}^{\infty} w(x) (\Phi_N(x) - \Phi(x))^2 d\Phi(x) \quad \text{where} \quad w(x) = \frac{1}{\Phi(x)(1 - \Phi(x))}.$$

A larger value of the distance A^2 means that it is less likely that the samples are coming from the proposed distribution with CDF Φ . The inference problem can be solved using the null hypothesis

$$H_0 : \xi \text{ follows a distribution with CDF } \Phi(x).$$

To assert the validity of the null hypothesis, we compute the so-called p -value, i.e., the probability that, under the proposed distribution in the null hypothesis, the value of A^2 is at least as large as the value of A^2 that was computed from the available samples. The null hypothesis H_0 is rejected only when this p -value is below a certain threshold, say 1%.

Let us repeat these steps for the three random variables $\tilde{\nu}$, $\tilde{\epsilon}$ and $\tilde{\chi}$, where we dropped the subscript $(\ell - 1, k)$ for convenience. The corresponding null hypotheses are

$$\begin{aligned} H_0^{\tilde{\nu}} : \tilde{\nu} \text{ follows a normal distribution with CDF } \Phi^{\mathcal{N}}(x), \text{ i.e., } \tilde{\nu} \sim \mathcal{N}(0, 1), \\ H_0^{\tilde{\epsilon}} : \tilde{\epsilon} \text{ follows an exponential distribution with CDF } \Phi^{\mathcal{E}}(x), \text{ i.e., } \tilde{\epsilon} \sim \mathcal{E}(1), \text{ and} \\ H_0^{\tilde{\chi}} : \tilde{\chi} \text{ follows a normal distribution with CDF } \Phi^{\mathcal{N}}(x), \text{ i.e., } \tilde{\chi} \sim \mathcal{N}(0, 1). \end{aligned} \tag{21}$$

Table 1 shows the AD distance A^2 and the p -value for background \mathbf{B}_1 with $a = 10$ and $b = 100$ for various (fine) levels ℓ , based on $N = 1000$ samples. The time step is given by $\delta t_\ell := T/2^\ell$ for the fine particle, and by $\delta t_{\ell-1} := M\delta t_\ell$ for the coarse particle. The entry $\ell = 5$ and $M = 2$, for example, means that we look for the random numbers $\tilde{\mathbf{y}}_4$ obtained from a coarsening of the random numbers \mathbf{y}_5 on level $\ell = 5$, with coarsening factor $M = 2$. All samples are obtained by running repeated particle simulations and recording all values for the (coarse particle) random numbers $\tilde{\epsilon}_{\ell-1,k}$, $\tilde{\nu}_{\ell-1,k}$ and $\tilde{\chi}_{\ell-1,k}$ for each collision $k = 0, \dots, \tilde{K}_{\ell_{j-1}}^{(n)}$, until $N = 1000$ realizations are available. We observe that in all cases, we fail to reject the null hypothesis, i.e., the p -value is above 0.01 (1%). Hence, we accept the hypotheses in equation (21), and find that the coarse aggregated random numbers satisfy the required distributions. A visual comparison of the exact CDF and its empirical counterpart in case $\ell = 5$ and $M = 2$ is shown in Figure 4 for all three random variables $\tilde{\nu}$, $\tilde{\epsilon}$ and $\tilde{\chi}$. Note that these results validate the telescopic sum in the multilevel estimator, i.e., equation (12): since \mathbf{y}_{ℓ_j} and $\tilde{\mathbf{y}}_{\ell_{j-1}}$ follow the same distribution, we have that

$$\mathbb{E}[Q_{\ell_{j-1}}(\mathbf{y}_{\ell_{j-1}})] = \mathbb{E}[Q_{\ell_{j-1}}(\tilde{\mathbf{y}}_{\ell_{j-1}})].$$

More results for background \mathbf{B}_2 and for all other parameter combinations can be found online at <https://>

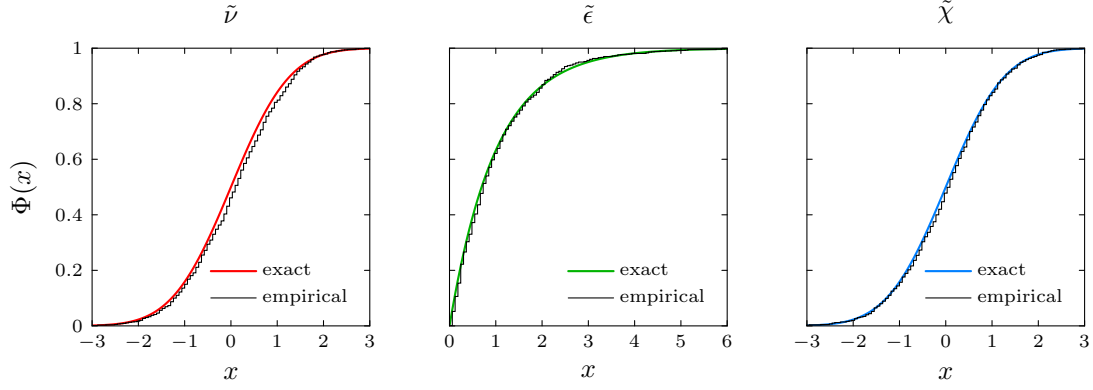


Figure 4: A visual comparison of the exact CDF and its empirical counterpart for the random variables $\tilde{\nu}$, $\tilde{\epsilon}$ and $\tilde{\chi}$ for background B_1 with $a = 10$, $b = 1\,000$, $\ell = 5$ and $K = 2$.

[//numa.cs.kuleuven.be/research_private/pieterjan.robbe/apmlmc/](http://numa.cs.kuleuven.be/research_private/pieterjan.robbe/apmlmc/).

5.2 A heuristic level selection method

Before we are able to use our ML-APMC method, we must specify which set of levels \mathcal{L} should be used. This is an important decision, since the choice of the level set \mathcal{L} determines the efficiency of the multilevel estimator (it appears directly in the expression for the cost of the multilevel estimator, equation (18)). Our strategy for selecting the optimal set of levels was outlined in Section 4.2. However, solving problem (20) for all combinations of collision rate parameters a and b would be computationally infeasible. Instead, we compute the optimal set of levels \mathcal{L}^* for a judiciously chosen set of parameter combinations with maximum level $L = 22$, and hope to devise some general guidelines for level selection for all other parameter combinations.

The effect of the level selection strategy can be visualized by inspecting the variances V_ℓ and $V_{\ell,\ell-1}$, $\ell = 0, 1, \dots, L$ and costs C_ℓ and $C_{\ell,\ell-1}$, $\ell = 0, 1, \dots, L$, see Figures 8–9. These figures indicate a similar behavior of the variance and cost of the multilevel difference for all parameter combinations, see the sketch in Figure 5

In the homogeneous case ($a = 0$, ---), the variance of the multilevel difference $V_{\ell,\ell-1}$ increases with decreasing time step δt_ℓ , until it reaches a maximum around $\delta t_\ell = 1/R(x)$. For even smaller values of

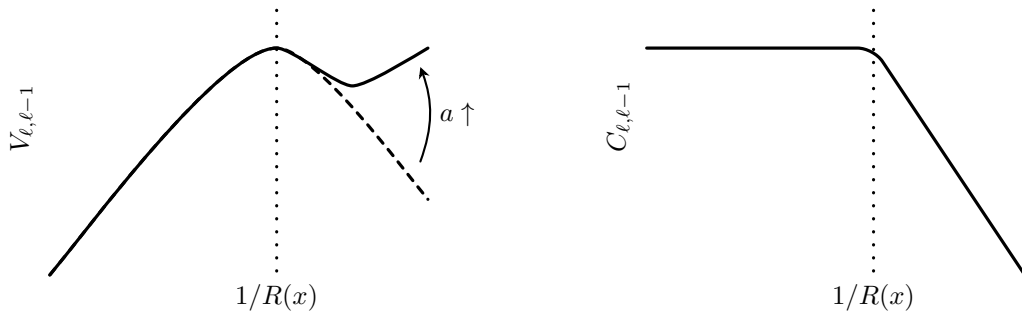


Figure 5: Behavior of variance (left) and cost (right) of the multilevel difference $\Delta Q_{\ell,\ell-1}$ with level ℓ . The homogeneous case ($a = 0$) is indicated by the dashed line (---), and the heterogeneous case ($a \gg 0$) is indicated by the full line (—).

		$M = 2$		$M = 4$		$M = 8$		$M = 16$		$M = 32$		$M = 64$	
		A^2	p	A^2	p	A^2	p	A^2	p	A^2	p	A^2	p
$\ell = 1$	$\tilde{\nu}$	0.344	0.902										
	$\tilde{\epsilon}$	0.622	0.627										
	$\tilde{\chi}$	0.207	0.988										
$\ell = 2$	$\tilde{\nu}$	0.171	0.996	0.656	0.597								
	$\tilde{\epsilon}$	0.352	0.895	0.397	0.852								
	$\tilde{\chi}$	0.385	0.863	0.691	0.566								
$\ell = 3$	$\tilde{\nu}$	0.286	0.948	0.422	0.827	0.265	0.962						
	$\tilde{\epsilon}$	0.553	0.693	0.574	0.673	0.427	0.822						
	$\tilde{\chi}$	0.165	0.997	0.364	0.884	0.554	0.692						
$\ell = 4$	$\tilde{\nu}$	0.329	0.915	0.626	0.624	0.440	0.809	0.602	0.646				
	$\tilde{\epsilon}$	0.415	0.834	0.296	0.941	1.088	0.314	0.483	0.764				
	$\tilde{\chi}$	0.362	0.885	0.242	0.974	0.440	0.808	0.310	0.930				
$\ell = 5$	$\tilde{\nu}$	0.261	0.964	0.258	0.966	0.693	0.565	0.629	0.621	0.251	0.970		
	$\tilde{\epsilon}$	0.131	1.000	0.826	0.463	0.196	0.991	0.574	0.673	0.512	0.735		
	$\tilde{\chi}$	0.277	0.954	0.402	0.847	0.166	0.997	0.425	0.824	0.611	0.637		
$\ell = 6$	$\tilde{\nu}$	0.550	0.696	0.286	0.948	0.473	0.774	0.433	0.816	0.414	0.835	0.416	0.833
	$\tilde{\epsilon}$	1.255	0.248	0.577	0.670	0.344	0.902	0.478	0.769	0.610	0.639	0.243	0.974
	$\tilde{\chi}$	0.290	0.945	0.813	0.472	0.301	0.938	0.260	0.965	0.671	0.583	0.271	0.958
$\ell = 7$	$\tilde{\nu}$	0.365	0.882	0.348	0.898	0.382	0.866	0.340	0.905	0.135	0.999	0.316	0.926
	$\tilde{\epsilon}$	0.648	0.604	0.254	0.968	1.299	0.233	0.426	0.822	0.282	0.951	0.413	0.836
	$\tilde{\chi}$	0.463	0.785	0.184	0.994	0.312	0.929	0.174	0.996	0.233	0.979	0.254	0.968
$\ell = 8$	$\tilde{\nu}$	0.682	0.574	0.252	0.969	0.416	0.833	0.250	0.970	0.641	0.610	0.103	1.000
	$\tilde{\epsilon}$	0.561	0.685	1.043	0.335	0.533	0.713	0.336	0.909	1.183	0.274	0.566	0.680
	$\tilde{\chi}$	0.179	0.995	0.707	0.553	0.325	0.918	0.511	0.736	0.253	0.969	0.295	0.942
$\ell = 9$	$\tilde{\nu}$	0.434	0.814	0.234	0.978	0.421	0.828	0.293	0.943	0.554	0.692	0.288	0.947
	$\tilde{\epsilon}$	0.748	0.520	0.560	0.687	0.305	0.935	0.200	0.991	0.545	0.702	0.408	0.841
	$\tilde{\chi}$	0.702	0.557	0.530	0.717	0.478	0.770	0.736	0.529	0.351	0.895	0.458	0.790
$\ell = 10$	$\tilde{\nu}$	0.312	0.929	0.563	0.684	0.215	0.986	0.628	0.622	0.644	0.607	0.633	0.618
	$\tilde{\epsilon}$	0.359	0.888	0.594	0.653	1.046	0.334	0.585	0.662	0.457	0.791	0.187	0.994
	$\tilde{\chi}$	0.234	0.978	0.376	0.873	0.194	0.992	0.301	0.938	0.294	0.943	0.343	0.903
$\ell = 11$	$\tilde{\nu}$	0.824	0.464	0.585	0.662	0.382	0.866	0.623	0.626	0.252	0.969	0.234	0.978
	$\tilde{\epsilon}$	0.637	0.614	0.438	0.810	0.332	0.912	0.567	0.680	1.101	0.309	0.307	0.932
	$\tilde{\chi}$	0.350	0.896	0.291	0.945	0.331	0.914	0.575	0.672	0.237	0.977	0.575	0.672
$\ell = 12$	$\tilde{\nu}$	0.258	0.966	0.717	0.545	0.206	0.989	0.483	0.764	0.412	0.836	0.250	0.970
	$\tilde{\epsilon}$	0.595	0.653	0.293	0.943	0.560	0.686	0.357	0.890	0.756	0.514	0.273	0.957
	$\tilde{\chi}$	0.265	0.962	0.481	0.767	0.252	0.969	0.243	0.974	0.300	0.938	0.748	0.520
$\ell = 13$	$\tilde{\nu}$	1.012	0.351	0.257	0.966	0.320	0.922	0.404	0.844	0.301	0.937	0.374	0.874
	$\tilde{\epsilon}$	0.790	0.488	0.709	0.552	1.787	0.121	0.418	0.831	0.477	0.770	0.458	0.789
	$\tilde{\chi}$	0.185	0.994	0.697	0.561	0.110	1.000	0.142	0.999	0.281	0.951	0.412	0.836
$\ell = 14$	$\tilde{\nu}$	0.632	0.618	0.389	0.860	0.355	0.892	0.584	0.663	0.265	0.962	0.584	0.664
	$\tilde{\epsilon}$	0.253	0.969	0.806	0.477	0.266	0.961	0.229	0.980	0.662	0.591	0.379	0.869
	$\tilde{\chi}$	0.557	0.690	0.126	1.000	0.296	0.941	0.360	0.887	0.235	0.978	0.150	0.999
$\ell = 15$	$\tilde{\nu}$	0.962	0.378	0.499	0.747	0.375	0.873	0.232	0.979	0.269	0.960	0.255	0.968
	$\tilde{\epsilon}$	0.333	0.912	0.561	0.685	0.421	0.827	0.356	0.891	0.608	0.641	0.258	0.966
	$\tilde{\chi}$	0.390	0.859	0.415	0.834	0.192	0.993	0.370	0.878	0.340	0.905	0.507	0.739

Table 1: Anderson–Darling distance A^2 and corresponding p -value for the aggregated coarse particle random numbers $\tilde{\epsilon}$, $\tilde{\nu}$ and $\tilde{\chi}$ for background B_1 with $a = 10$ and $b = 1\,000$ and various levels $\ell = 1, 2, \dots, 15$ and level multiplication factors $M \in \{2, 4, 8, 16, 32, 64\}$ based on $N = 1\,000$ samples. The random numbers do not follow the required distributions (i.e., the null hypothesis is rejected) when the p -value is below 0.01.

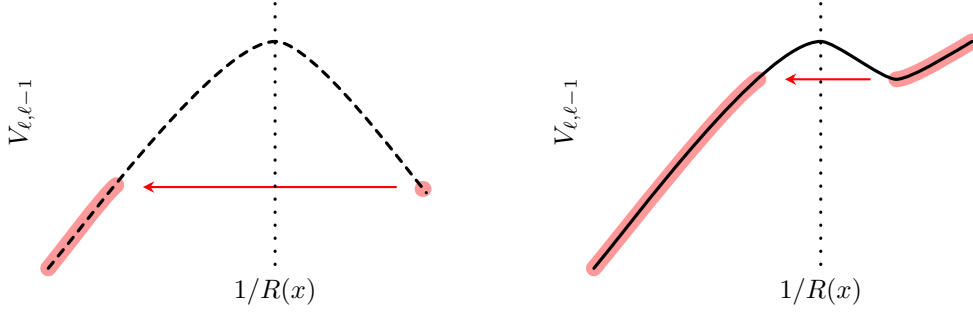


Figure 6: Summary of the level selection strategy from Section 4.2 for a homogeneous (*left*) and heterogeneous (*right*) background. Levels indicated by \bullet are selected for the optimal level set \mathcal{L}^* .

the time step δt_ℓ , the variance decreases at a rate proportional to $\mathcal{O}(\delta t_\ell^3)$. As the heterogeneity increases ($a \uparrow$, ---), there is an additional error that decays as $\mathcal{O}(\delta t_\ell)$, which makes the variance of the multilevel difference decay to a local minimum before it increases again. We remark that the behavior for $b = 1$ and $b = 10$ in Figure 8 is a degenerate case of the more general behavior sketched above, where the local maximum is shifted to the right, outside the range of available time step sizes. The computational cost $C_{\ell, \ell-1}$ in Figure 9 increases linearly with δt_ℓ until the local maximum in the variance decay curve is reached, after which the cost scales independent of the time step. This behavior is consistent with the error analysis of the APMC scheme in [19]: For large values of the time step size δt_ℓ , the scheme converges to the diffusive approximation of the Boltzmann-BGK equation, while for small values of δt_ℓ , the scheme converges to the kinetic approximation (i.e., the direct simulation of each collision of the particle).

For our APMC scheme, the level selection strategy from Section 4.2 can be summarized as in Figure 6. Given the variance V_ℓ for each $\ell = 0, 1, \dots, L$, and the variance of the multilevel difference $V_{\ell, \ell-1}$ for each $\ell = 1, 2, \dots, L$, the set of levels \mathcal{L} can be selected heuristically using Algorithm 3. This approach has several advantages. First of all, there is no need to compute the solution of the integer linear programming problem from equation (20) for every new background collision rate parameter combination. Furthermore, the required quantities V_ℓ and $V_{\ell, \ell-1}$ can be approximated by the sample variance of a set of (cheap) warm-up samples for levels ℓ where $\delta t_\ell \geq 1/R(x)$, and we can use the asymptotic complexity rate of $V_{\ell, \ell-1}$ for all other levels ℓ where $\delta t_\ell < 1/R(x)$. The warm-up samples for every level $\ell \in \mathcal{L}$ can be reused to hot start the multilevel estimator. Also, our approach is level-adaptive: increasing the maximum level parameter L does not force us to recompute the level set \mathcal{L} . Finally, the subsequent level sets \mathcal{L} are nested for different L , which means that no computational effort is wasted when L is increased. This would be the case if a particular level ℓ is part of the set \mathcal{L} for the maximum level parameter L , but is not a part of the set \mathcal{L} for the maximum level parameter $L + 1$.

5.3 Performance of the ML-APMC method

In this section, we compare the efficiency of the new ML-APMC scheme to the efficiency of the standard, single-level APMC scheme in terms of error (ε) versus computational work (wall clock time). We will show numerically that both the single-level and multilevel method have an asymptotic ε -cost complexity of $\mathcal{O}(\varepsilon^{-2})$, i.e., the expected complexity of an MC-based method, but the constant is significantly reduced for the multilevel scheme. Every experiment consists of an off-line and an on-line part. The off-line part starts by taking $N_{\text{warm-up}}$ warm-up samples on each level $\ell = 0, 1, \dots, \tau$, where τ is such that $\delta t_\tau \approx 1/b$, with b the constant parameter in the background collision rate. In our numerical

Algorithm 3: Heuristic level selection approach.

input: estimates for the variances V_ℓ , $\ell = 0, 1, \dots, L$ and $V_{\ell, \ell-1}$, $\ell = 1, 2, \dots, L$
output: a set of levels $\mathcal{L} = \{\ell_j\}_{j=1}^J$

```

1: procedure level_select( $V_0, V_1, \dots, V_L, V_{1,0}, V_{2,1}, \dots, V_{L,L-1}$ )
2:    $\ell \leftarrow 1$ 
3:   while  $V_{\ell, \ell-1} > V_\ell$  do                                     // find first level  $\ell$  where  $V_{\ell, \ell-1} < V_\ell$ 
4:      $\ell \leftarrow \ell + 1$ 
5:   end while
6:    $\mathcal{L} \leftarrow \{\ell - 1, \ell\}$                                    // a minimum of 2 levels is required for MLMC
7:    $V_{\min} \leftarrow V_{\ell, \ell-1}$ 
8:   for  $\ell = 0, 1, \dots, L$  do
9:     if  $V_{\ell, \ell-1} < V_{\min}/2$  then // only add level  $\ell$  if sufficient variance decay in  $V_{\ell, \ell-1}$ 
10:       $\mathcal{L} \leftarrow \mathcal{L} \cup \{\ell\}$ 
11:       $V_{\min} \leftarrow V_{\ell, \ell-1}$ 
12:    end if
13:  end for
14:  return  $\mathcal{L}$ 
15: end procedure

```

experiments, we used $N_{\text{warm-up}} = 100$. From this set of warm-up samples, we compute the variances V_ℓ , $\ell = 0, 1, \dots, L$ and $V_{\ell, \ell-1}$, $\ell = 1, 2, \dots, L$, where the values $V_{\ell, \ell-1}$ with $\ell < \tau$ are approximated by the sample variance using the $N_{\text{warm-up}}$ warm-up samples, and the values $V_{\ell, \ell-1}$ with $\ell > \tau$ are estimated using the asymptotic ratio $V_{\ell, \ell-1} = \mathcal{O}(\delta t_\ell^3)$. These variances are then used as input for the level selection algorithm, i.e., Algorithm 3. It should be stressed that the amount of computational work of this off-line setup phase is orders of magnitude less than the on-line phase, described below.

In the on-line phase, we run the (single-level) APMC and multilevel APMC algorithm repeatedly for a decreasing sequence of tolerances $\varepsilon^{(r)} = 1/\sqrt{2^r}$ for $r = 0, 1, 2, \dots, R$ imposed on the RMSE. The value R is determined such that the APMC scheme runs for approximately 10 000s (wall clock time), and the value $\sqrt{2}$ is such that each simulation takes about twice the amount of work of the previous iteration, assuming the ε -cost complexity of the method scales as $\mathcal{O}(\varepsilon^{-2})$. The main reason for this ε -adaptive strategy is that it yields more reliable estimates of the bias $|\mathbb{E}[Q_L - Q]|$, see, e.g., [6, 25] for details.

Figure 7(a) shows the asymptotic ε -complexity of the ML-APMC and (single-level) APMC method for background B_1 with $a = 10$ and $b = 1000$. Note that both methods indeed follow the asymptotic cost complexity $\mathcal{O}(\varepsilon^{-2})$. However, the cost of the multilevel method is significantly reduced. Next, in Figure 7(b) we show the total number of samples N_{ℓ_j} , $j = 1, 2, \dots, J$, in the multilevel method for different values of the tolerance ε for background B_1 with $a = 10$ and $b = 100$. Note that these values are decreasing with increasing j . Hence, most samples will be taken with a large time step δt_{ℓ_1} , and fewer and fewer samples are required with smaller time step sizes, as claimed in Section 4.1. Again, we refer to https://numa.cs.kuleuven.be/research_private/pieterjan.robbe/apmlmc/ for results including all other parameter combinations.

Next, in Table 2, we report the algorithmic speedup (computed as the ratio of the amount of computational work expressed in wall clock time) of our ML-APMC method compared to APMC for both backgrounds B_1 and B_2 , and for all background parameter values a and b . We note that the MLMC method performs better for larger values of b (i.e., the constant in the background collision rates $R_1(x)$ and $R_2(x)$). The performance decreases slightly with increasing heterogeneity (larger values of a). We remark that, in a practical setting, one is interested in large values of the collision rate (large b) and moderate to large amounts of heterogeneity (moderate to large values of a). We expect our ML-APMC

method to perform exceptionally well in these cases.

6 Conclusion and future work

In this paper, we introduced the multilevel extension of the Asymptotic-Preserving Monte Carlo (APMC) scheme for solving the Boltzmann-BGK equation proposed in [19]. Crucial in our algorithm is the new and improved recipe for correlated sampling of a particle trajectory with different time step sizes. We show that this correlated sampling can be achieved using a mapping and aggregation strategy for the random numbers used in the particle path simulation. We also discussed specific challenges in applying the multilevel sampling strategy to the APMC scheme. Notably, because of the nonmonotone behavior of the variance and cost of the multilevel differences, the selection of the appropriate hierarchy of larger time step sizes becomes a nontrivial problem. We introduced a heuristic method for this level selection problem, that avoids solving a combinatorial optimization problem involving all possible combinations of larger time step sizes. We illustrate numerically that our new ML-APMC scheme with optimal level hierarchy outperforms the classic, single-level APMC scheme in terms of error versus computational cost by several orders of magnitude, for a wide variety of background collision rate parameter combinations. The implementation of the (ML-)APMC scheme in actual nuclear fusion plasma simulation codes, such as EIRENE [24], is the topic of currently ongoing research.

Future work may also focus on devising a Multilevel Monte Carlo (MLMC) cost complexity theorem that covers the APMC case, taking into account the specific behavior of the variance and cost of the multilevel differences (Figures 8 and 9). The APMC scheme from [19] could also be extended by using an improved sampling method, such as *Quasi-Monte Carlo* (QMC), using techniques from the SDE literature, see, e.g., [14]. The resulting *Asymptotic-Preserving Quasi-Monte Carlo* APQMC scheme could then be straightforwardly extended to a *Multilevel Asymptotic-Preserving Quasi-Monte Carlo* (ML-APQMC) scheme, offering both a faster convergence (a cost complexity $\mathcal{O}(\varepsilon^{-1})$, due to the QMC method) and a reduced constant.

Finally, we remark that our ML-APMC simulation scheme is not limited to the kinetic simulation of the Boltzmann-BGK equation in nuclear fusion. Applications in, amongst others, rarefied gases, see [22], and radiation transport, see [10], can benefit from our hybrid (ML-)APMC method. This will be the topic of a future publication.

References

- [1] APPEGATE, D. L., BIXBY, R. E., CHVATAL, V., AND COOK, W. J. *The Traveling Salesman Problem: a Computational Study*. Princeton University Press, 2006.
- [2] BHATNAGAR, P. L., GROSS, E. P., AND KROOK, M. A Model for Collision Processes in Gases. I. Small Amplitude Processes in Charged and Neutral One-Component Systems. *Physical review* 94, 3 (1954), 511.
- [3] BÖRGERS, C., LARSEN, E. W., AND ADAMS, M. L. The Asymptotic Diffusion Limit of a Linear Discontinuous Discretization of a Two-dimensional Linear Transport Equation. *Journal of Computational Physics* 98, 2 (1992), 285–300.

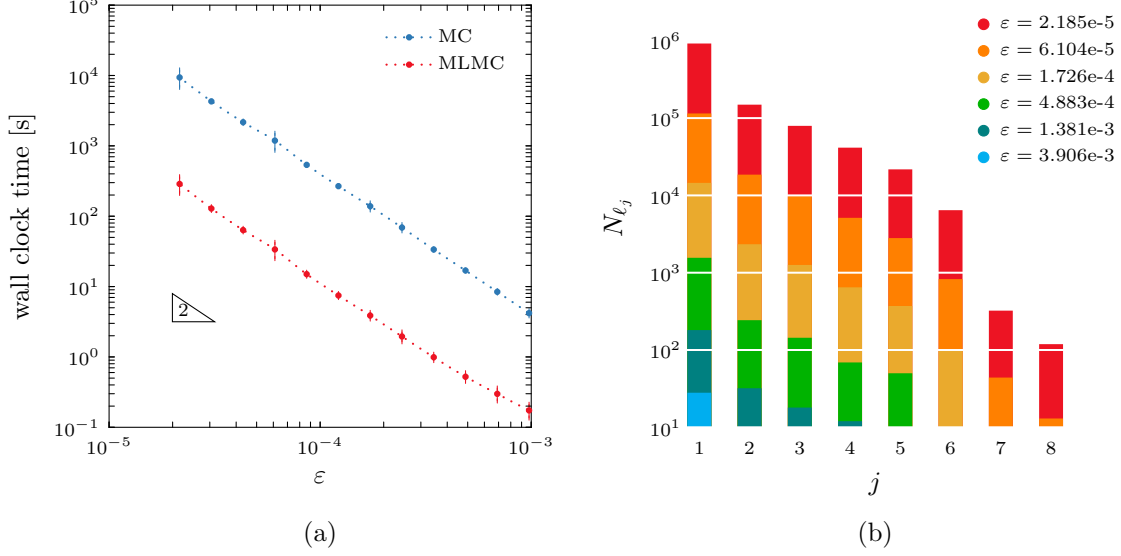


Figure 7: (a) Cost complexity of ML-APMC and APMC for background B_1 with $a = 10$ and $b = 1000$. (b) Total number of samples on each level $\ell_j \in \mathcal{L}$, $j = 1, 2, \dots, 8$ for background B_1 with $a = 10$ and $b = 1000$.

	$b = 1$	$b = 10$	$b = 100$	$b = 1000$	$b = 10000$	$b = 100000$
$a = 0$	1.19 ± 0.10	2.22 ± 0.00	20.29 ± 0.06	148.43 ± 0.81	1511.89 ± 48.49	22276.16 ± 1206.11
$a = 0.1$	1.22 ± 0.10	2.49 ± 0.00	20.80 ± 2.00	162.62 ± 0.66	1196.21 ± 20.34	14076.73 ± 311.93
$a = 0.2$	1.19 ± 0.01	2.56 ± 0.00	21.36 ± 1.17	162.31 ± 0.82	1203.30 ± 13.26	11931.86 ± 242.94
$a = 0.5$	1.17 ± 0.01	2.72 ± 0.01	21.48 ± 0.26	118.98 ± 0.41	1000.70 ± 5.52	11929.95 ± 187.13
$a = 1$	1.14 ± 0.01	2.68 ± 0.01	17.63 ± 0.07	120.35 ± 0.19	1000.87 ± 5.98	7589.55 ± 168.20
$a = 2$	1.14 ± 0.01	2.81 ± 0.01	17.25 ± 0.02	102.70 ± 0.25	638.25 ± 1.63	9236.13 ± 131.17
$a = 5$	1.18 ± 0.02	2.35 ± 0.01	15.38 ± 0.03	85.42 ± 0.15	642.67 ± 1.88	9133.13 ± 142.74
$a = 10$	1.21 ± 0.02	1.87 ± 0.01	14.54 ± 0.01	80.79 ± 0.14	499.99 ± 1.73	6766.04 ± 102.58
$a = 20$	1.35 ± 0.06	2.04 ± 0.01	17.74 ± 0.03	74.09 ± 0.10	497.18 ± 2.70	7636.25 ± 81.69
$a = 50$	1.15 ± 0.05	2.43 ± 0.02	9.98 ± 0.02	84.74 ± 0.15	457.36 ± 2.37	4684.73 ± 77.78
$a = 100$	1.23 ± 0.03	2.61 ± 0.04	8.69 ± 0.05	122.60 ± 0.66	452.88 ± 7.57	3056.32 ± 27.19

Table 2: Algorithmic speedup of the ML-APMC method (compared to single-level APMC) for background B_1 and various background parameters a and b . A green background color (●) is a speedup, a red background color (●) is a slowdown. Color saturation indicates the amount of speedup or slowdown.

	$b = 1$	$b = 10$	$b = 100$	$b = 1000$	$b = 10000$	$b = 100000$
$a = 0$	1.19 ± 0.09	2.22 ± 0.01	21.29 ± 0.04	149.07 ± 0.34	1438.15 ± 33.72	21271.88 ± 1120.02
$a = 0.1$	1.23 ± 0.11	2.40 ± 0.01	20.84 ± 0.02	157.45 ± 0.82	1629.46 ± 26.07	14279.19 ± 566.27
$a = 0.2$	1.19 ± 0.00	2.55 ± 0.00	21.53 ± 0.05	156.41 ± 0.74	1576.88 ± 36.40	14547.13 ± 473.81
$a = 0.5$	1.18 ± 0.00	2.57 ± 0.00	23.23 ± 0.04	158.20 ± 0.83	1127.70 ± 13.89	11875.57 ± 147.67
$a = 1$	1.14 ± 0.01	2.67 ± 0.00	21.58 ± 0.02	118.54 ± 0.28	991.45 ± 7.17	7446.33 ± 135.31
$a = 2$	1.16 ± 0.02	2.66 ± 0.00	19.91 ± 0.05	111.60 ± 0.36	986.87 ± 5.98	9181.21 ± 142.87
$a = 5$	1.41 ± 0.16	2.67 ± 0.00	17.10 ± 0.02	92.69 ± 0.23	632.20 ± 1.71	9352.35 ± 160.51
$a = 10$	1.17 ± 0.01	2.40 ± 0.00	14.43 ± 0.01	66.72 ± 0.07	635.49 ± 2.81	9250.00 ± 161.89
$a = 20$	1.00 ± 0.04	2.41 ± 0.02	14.24 ± 0.01	80.74 ± 0.11	505.88 ± 1.49	8605.50 ± 133.31
$a = 50$	1.25 ± 0.00	1.82 ± 0.05	15.26 ± 0.03	70.84 ± 0.13	484.00 ± 2.07	6159.53 ± 136.14
$a = 100$	1.00 ± 0.00	1.68 ± 0.01	18.99 ± 0.07	66.06 ± 0.13	450.02 ± 4.35	5019.00 ± 107.72

Table 2 (continued): Algorithmic speedup of the ML-APMC method (compared to single-level APMC) for background B_2 and various background parameters a and b . A green background color (●) is a speedup, a red background color (●) is a slowdown. Color saturation indicates the amount of speedup or slowdown.

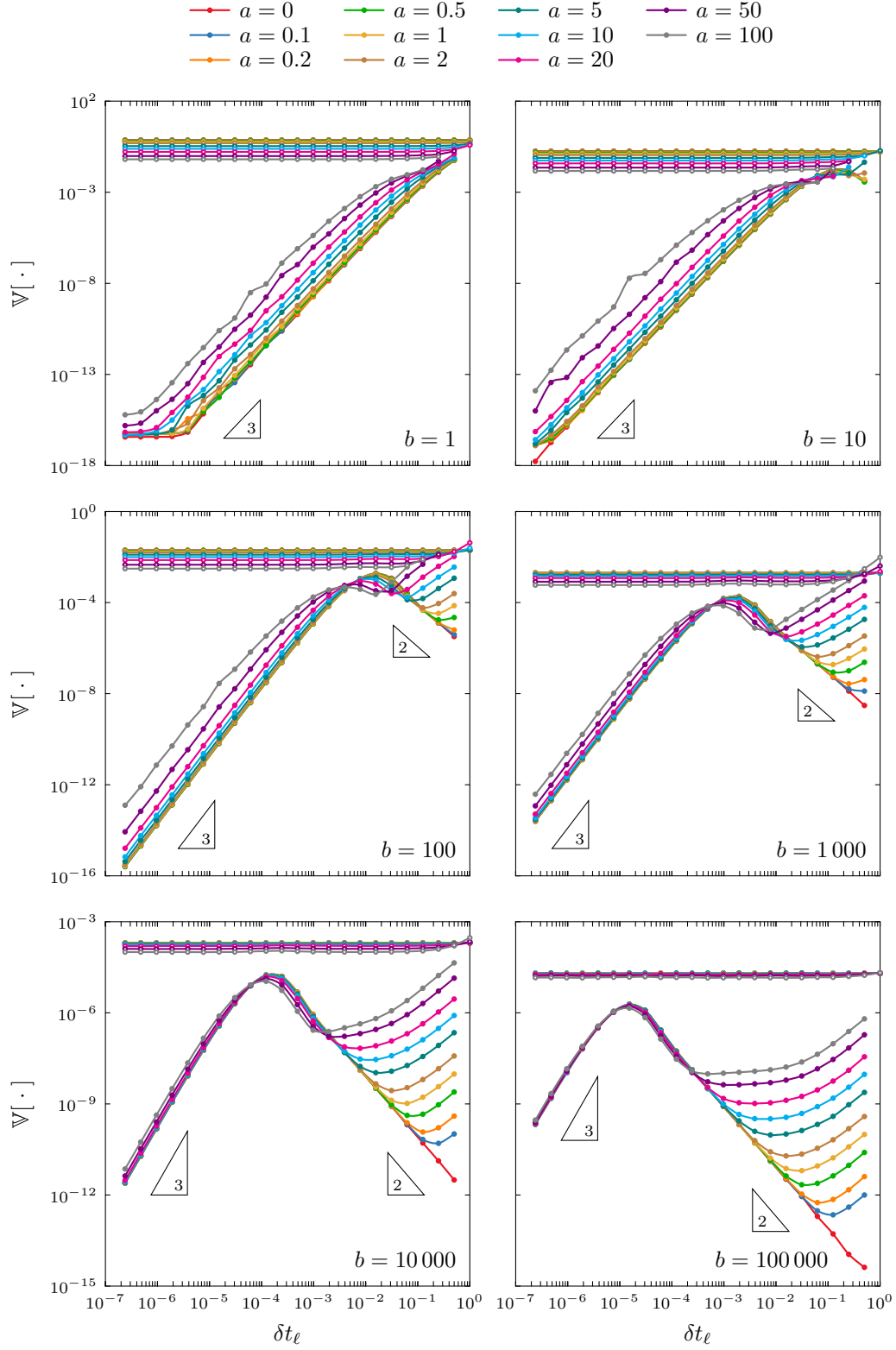


Figure 8: Behavior of the variances $V_\ell = \mathbb{V}[Q_\ell]$ (\circ) and $V_{\ell,\ell-1} = \mathbb{V}[Q_\ell - Q_{\ell-1}]$ (\bullet) for background B_1 for different values of the parameters a and b . Results obtained for 10^6 particles for $b = 1$ and $b = 10$, 10^5 particles for $b = 100$ and $b = 1000$ and 10^4 particles for $b = 10000$ and $b = 100000$.

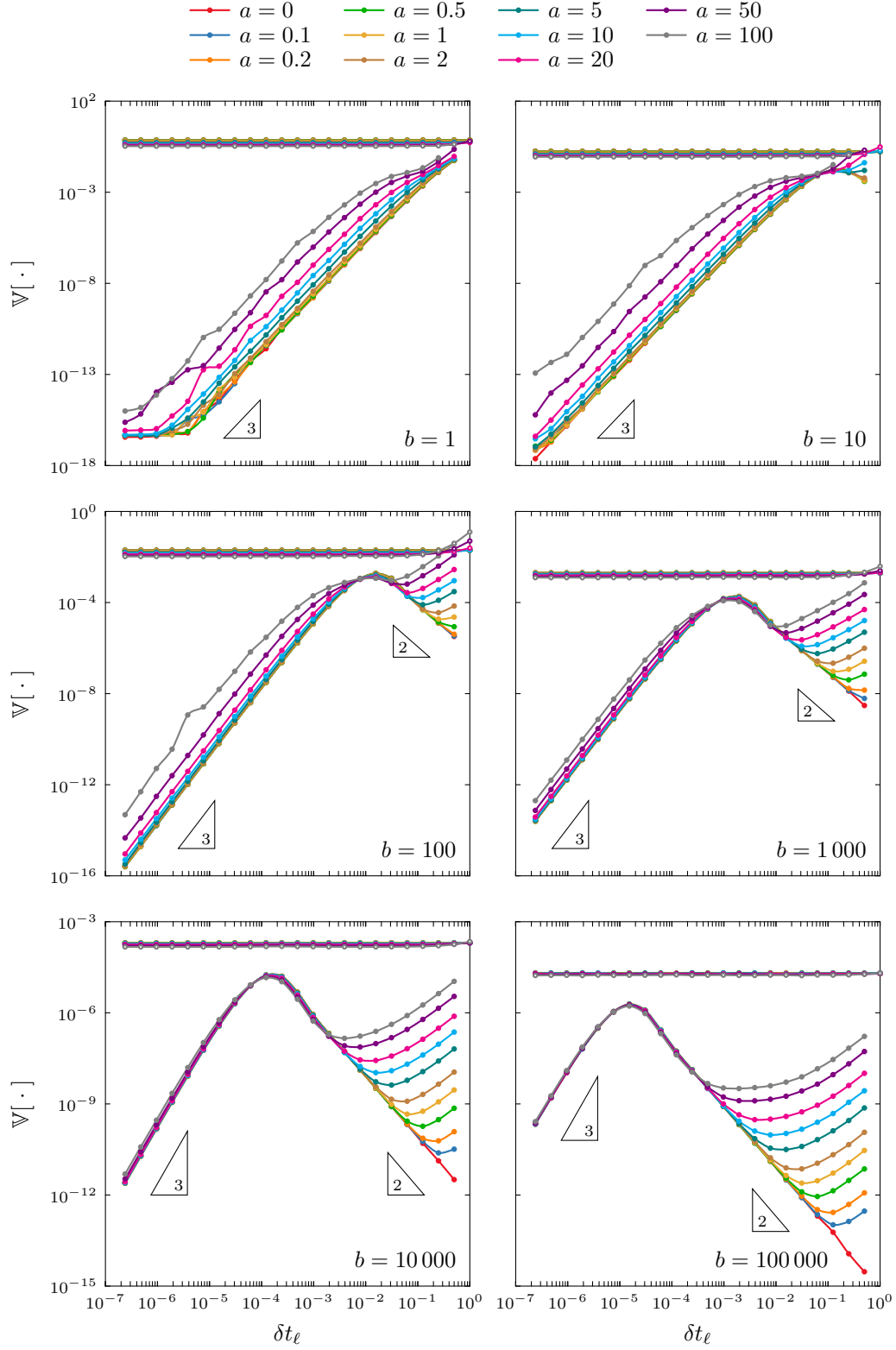


Figure 8 (continued): Behavior of the variances $V_\ell = \mathbb{V}[Q_\ell]$ (\circ) and $V_{\ell,\ell-1} = \mathbb{V}[Q_\ell - Q_{\ell-1}]$ (\bullet) for background B_2 for different values of the parameters a and b . Results obtained for 10^6 particles for $b = 1$ and $b = 10$, 10^5 particles for $b = 100$ and $b = 1000$ and 10^4 particles for $b = 10000$ and $b = 100000$.

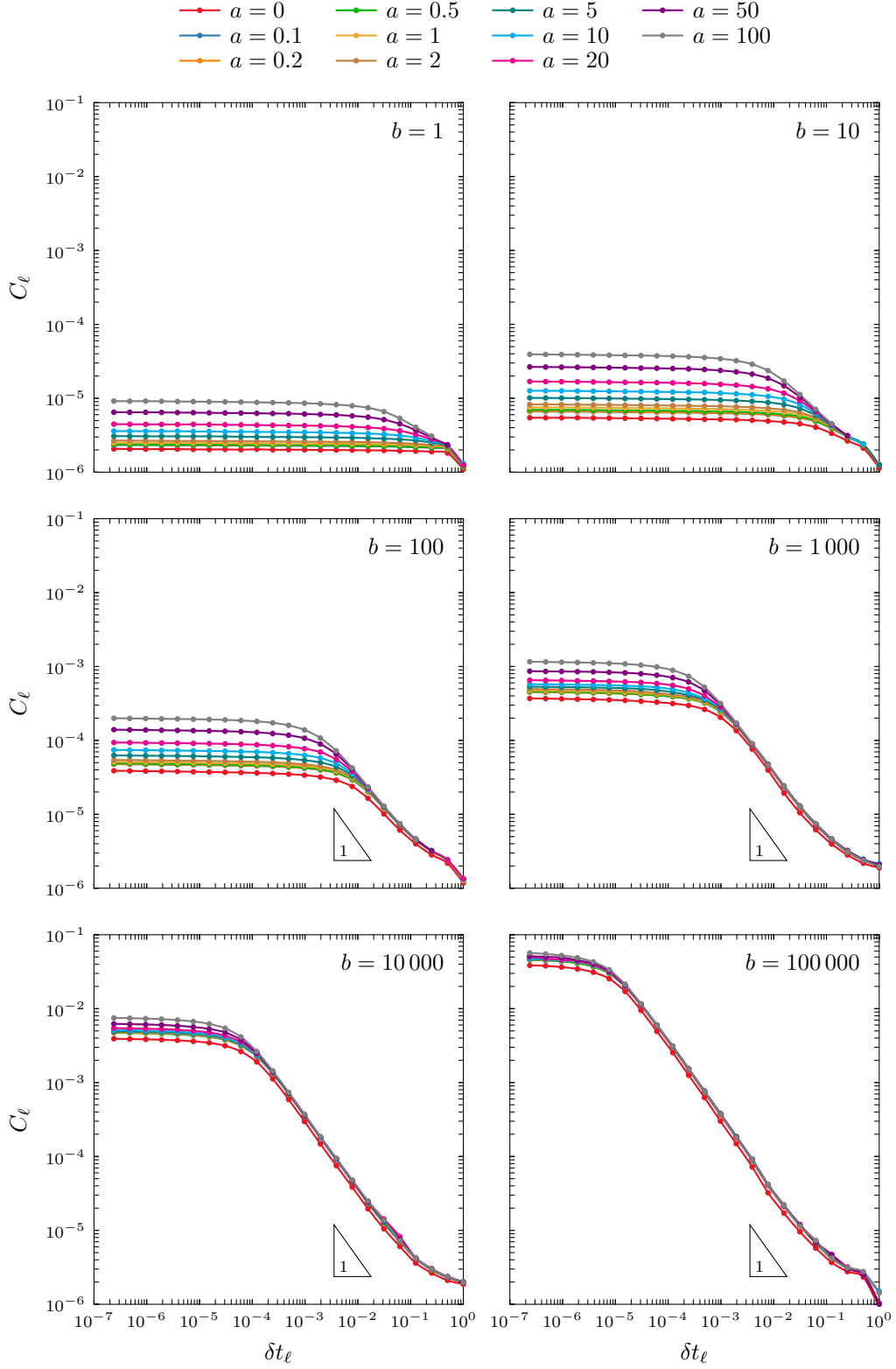


Figure 9: Behavior of the cost $C_\ell = \mathcal{C}(Q_{\ell, \ell-1})$ for background B_1 for different values of the parameters a and b . Results obtained for 10^6 particles for $b = 1$ and $b = 10$, 10^5 particles for $b = 100$ and $b = 1000$ and 10^4 particles for $b = 10000$ and $b = 100000$.

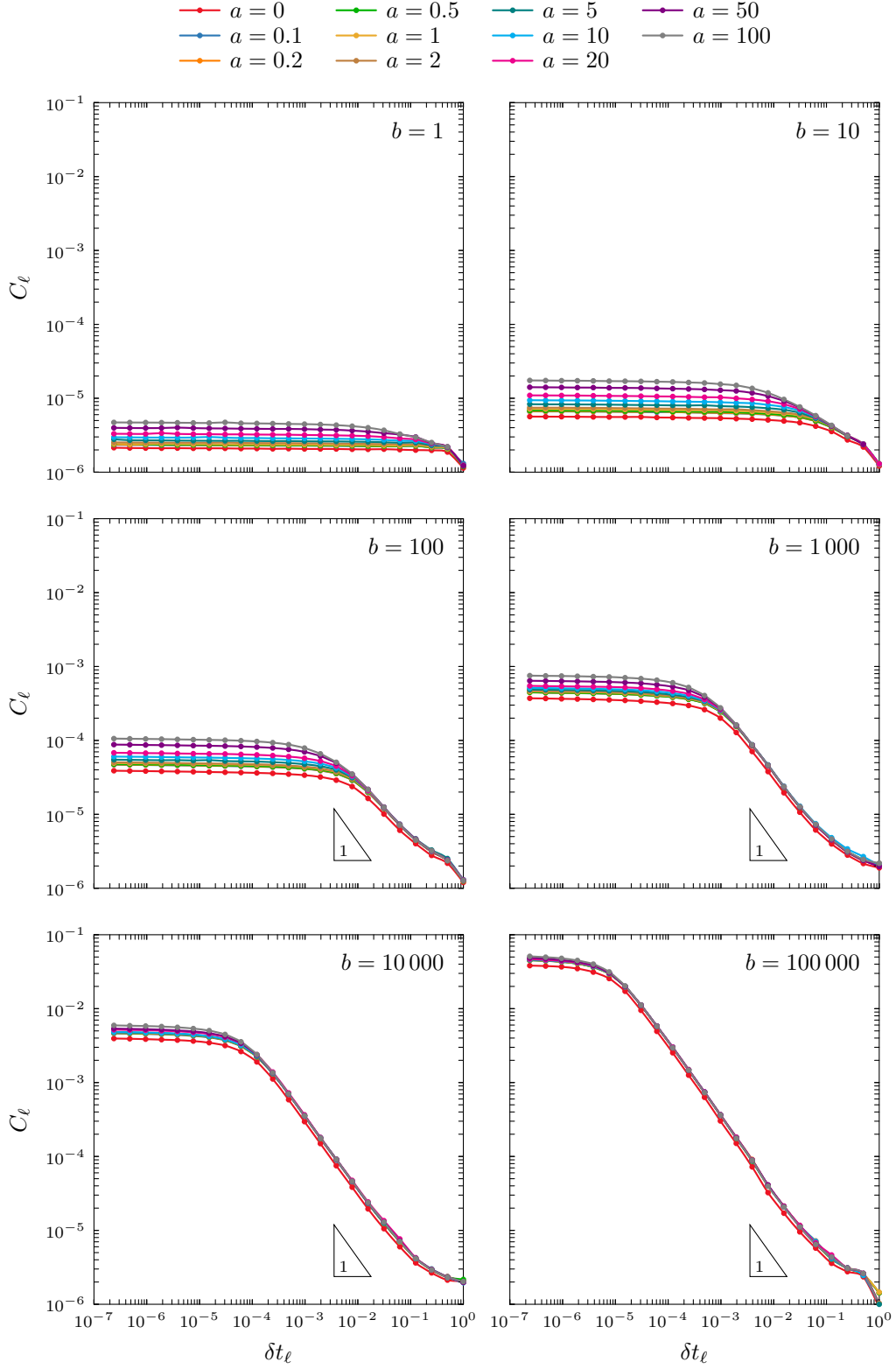


Figure 9 (continued): Behavior of the cost $C_\ell = \mathcal{C}(Q_{\ell, \ell-1})$ for background B_2 for different values of the parameters a and b . Results obtained for 10^6 particles for $b = 1$ and $b = 10$, 10^5 particles for $b = 100$ and $b = 1000$ and 10^4 particles for $b = 10000$ and $b = 100000$.

- [4] BOYD, I. D., AND DESCHENES, T. R. Hybrid Particle-Continuum Numerical Methods for Aerospace Applications, Technical Report, DTIC document. Tech. rep., Michigan Univ Ann Arbor Dept of Aerospace Engineering, 2011.
- [5] CLIFFE, K. A., GILES, M. B., SCHEICHL, R., AND TECKENTRUP, A. L. Multilevel Monte Carlo Methods and Applications to Elliptic PDEs with Random Coefficients. *Computing and Visualization in Science* 14, 1 (2011), 3–15.
- [6] COLLIER, N., HAJI-ALI, A.-L., NOBILE, F., SCHWERIN, E., AND TEMPONE, R. A Continuation Multilevel Monte Carlo Algorithm. *BIT Numerical Mathematics* 55, 2 (2014), 399–432.
- [7] DENSMORE, J. D., URBATSCH, T. J., EVANS, T. M., AND BUKSAS, M. W. A Hybrid Transport-Diffusion Method for Monte Carlo Radiative-Transfer Simulations. *Journal of Computational Physics* 222, 2 (2007), 485–503.
- [8] DIMARCO, G., PARESCHI, L., AND SAMAHEY, G. Asymptotic-Preserving Monte Carlo Methods for Transport Equations in the Diffusive Limit. *SIAM Journal on Scientific Computing* 40, 1 (2018), A504–A528.
- [9] FLECK JR, J., AND CANFIELD, E. A Random Walk Procedure for Improving the Computational Efficiency of the Implicit Monte Carlo Method for Nonlinear Radiation Transport. *Journal of Computational Physics* 54, 3 (1984), 508–523.
- [10] FLECK JR, J., AND CUMMINGS JR, J. An Implicit Monte Carlo Scheme for Calculating Time and Frequency Dependent Nonlinear Radiation Transport. *Journal of Computational Physics* 8, 3 (1971), 313–342.
- [11] GABETTA, E., PARESCHI, L., AND TOSCANI, G. Relaxation Schemes for Nonlinear Kinetic Equations. *SIAM Journal on Numerical Analysis* 34, 6 (1997), 2168–2194.
- [12] GILES, M. B. Multilevel Monte Carlo Path Simulation. *Operations Research* 56, 3 (2008), 607–617.
- [13] GILES, M. B. Multilevel Monte Carlo Methods. *Acta Numerica* 24 (2015), 259–328.
- [14] GILES, M. B., AND WATERHOUSE, B. J. Multilevel Quasi-Monte Carlo Path Simulation. *Advanced Financial Modelling, Radon Series on Computational and Applied Mathematics* (2009), 165–181.
- [15] ITER: International Thermonuclear Experimental Reactor. Online, url: <https://www.iter.org>. Accessed on 2020-04-03.
- [16] LØVBAK, E., SAMAHEY, G., AND VANDEWALLE, S. A Multilevel Monte Carlo Method for Asymptotic-Preserving Particle Schemes. *ArXiv preprint* (2019).
- [17] LUX, I., AND KOBLINGER, L. *Monte Carlo Particle Transport Methods: Neutron and Photon Calculations*. CRC Press, Cleveland, Ohio, 1991.
- [18] MORTIER, B., BAELEMAN, M., AND SAMAHEY, G. Kinetic-diffusion asymptotic-preserving monte carlo algorithms for plasma edge neutral simulation. *Contributions to Plasma Physics* (2019), 1–6.
- [19] MORTIER, B., BAELEMAN, M., AND SAMAHEY, G. Kinetic-Diffusion Asymptotic-Preserving Monte Carlo Algorithm for Boltzmann-BGK in the Diffusive Scaling. *ArXiv preprint* (2020).
- [20] OTHMER, H. G., AND HILLEN, T. The Diffusion Limit of Transport Equations derived from Velocity-Jump Processes. *SIAM Journal on Applied Mathematics* 61, 3 (2000), 751–775.
- [21] PADBERG, M., AND RINALDI, G. A Branch-and-Cut Algorithm for the Resolution of Large-scale Symmetric Traveling Salesman Problems. *SIAM review* 33, 1 (1991), 60–100.

- [22] PARESCHI, L., AND CAFLISCH, R. E. An Implicit Monte Carlo Method for Rarefied Gas Dynamics: I. The Space Homogeneous Case. *Journal of Computational Physics* 154, 1 (1999), 90–116.
- [23] PARESCHI, L., AND RUSSO, G. Time-Relaxed Monte Carlo Methods for the Boltzmann Equation. *SIAM Journal on Scientific Computing* 23, 4 (2001), 1253–1273.
- [24] REITER, D., BAELMANS, M., AND BØRNER, P. The EIRENE and B2-EIRENE Codes. *Fusion Science and Technology* 47, 2 (2005), 172–186.
- [25] ROBBE, P., NUYENS, D., AND VANDEWALLE, S. A Multi-Index Quasi-Monte Carlo Algorithm for Lognormal Diffusion Problems. *SIAM Journal on Scientific Computing* 39, 5 (2017), S851–S872.
- [26] STANGEBY, P. C. *The Plasma Boundary of Magnetic Fusion Devices*. CRC Press, Cleveland, Ohio, 2000.